

In-Context Bias Propagation in LLM-Based Tabular Data Generation

Pol G. Recasens^{a,*}, Alberto Gutierrez^a, Jordi Torres^{a,b}, Josep Ll. Berral^{b,a}, Javier Carnerero-Cano^c, Anisa Halimi^c, Kieran Fraser^c

^aBarcelona Supercomputing Center (BSC), Spain
^bUniversitat Politècnica de Catalunya (UPC), Spain
^cIBM Research Ireland

Abstract

Large Language Models (LLMs) are increasingly used for synthetic tabular data generation through in-context learning (ICL), offering a practical solution for data augmentation in data scarce scenarios. While prior work has shown the potential of LLMs to improve downstream task performance through augmenting underrepresented groups, these benefits often assume access to a subset of unbiased in-context examples, representative of the real dataset. In real-world settings, however, data is frequently noisy and demographically skewed. In this paper, we systematically study how statistical biases within in-context examples propagate to the distribution of synthetic tabular data, showing that even mild in-context biases lead to global statistical distortions. We further introduce an adversarial scenario where a malicious contributor can inject bias into the synthetic dataset via a subset of in-context examples, ultimately compromising the fairness of downstream classifiers for a targeted and protected subgroup. Finally, we evaluate mitigation strategies based on preprocessing in-context examples, demonstrating that while such interventions can attenuate disparity, the inherent sensitivity of LLMs to adversarial prompts remains a persistent challenge. Our findings highlight a critical new vulnerability in LLM-based data generation pipelines within sensitive domains.

Keywords: in-context learning, bias mitigation, synthetic data generation, large language models

1. Introduction

The scarcity of high-quality, labeled data remains a primary bottleneck in deploying machine learning systems in sensitive domains such as healthcare, finance, and criminal justice. Due to strict privacy regulations and the high cost of manual annotation, practitioners increasingly rely on synthetic data augmentation to build robust classifiers [1]. While traditional generative models [2, 3] have been the standard for tabular synthesis, they often require substantial in-domain data to generate reliable data.

Recently, Large Language Models (LLMs) have emerged as a powerful alternative, demonstrating remarkable generalization capabilities through in-context learning (ICL). By conditioning on a small set of ICL examples, LLMs can generate realistic, statistically coherent tabular samples without the need for fine-tuning [1]. This paradigm leverages the model’s strong semantic priors to augment underrepresented groups, offering a resource-efficient solution for data-scarce regimes. Recent studies show that LLM-generated synthetic data can significantly boost downstream task performance, matching or even surpassing traditional data augmentation methods in data-scarce regimes [4, 5].

However, the efficacy of ICL relies on a critical and often unexamined assumption, which is that in-context examples provided in the prompt are unbiased and independently drawn from the real data distribution. In real-world deployment scenarios –such as Retrieval-Augmented Generation (RAG) pipelines or collaborative data platforms –this assumption rarely holds. In-

context examples are frequently noisy, skewed, or dynamically retrieved from unverified sources.

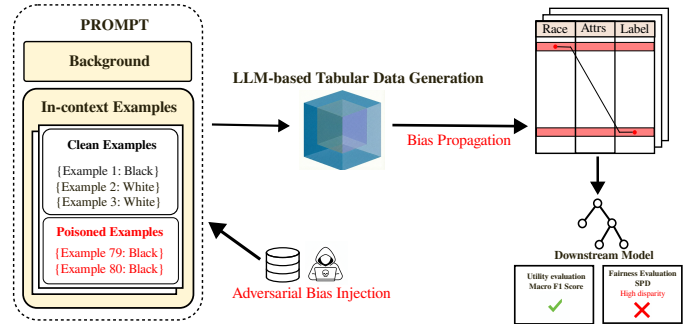


Figure 1: **End-to-end bias propagation.** An adversarial user injects biased examples into the prompt for a targeted group. The LLM replicates these statistical patterns via in-context learning, propagating the bias into the synthetic tabular data, and further compromising downstream fairness.

This paper addresses *in-context bias propagation*, a critical vulnerability inherent to LLM-based synthetic data generation. Unlike traditional “intrinsic” bias, which stems from the model’s pretraining weights [6], we investigate “extrinsic” bias introduced at inference time, noting that in practice, these two source of bias interact during generation. We argue that the same mechanism that allows LLMs to adapt rapidly to new tasks also makes them susceptible to replicating and amplifying demographic disparities present in the context examples. Consider a community hospital utilizing an LLM to augment a dataset where patient records disproportionately represent a specific demographic. As illustrated in Figure 1, such statistical imbalances can inadver-

*Corresponding author: pol.garcia@bsc.es

tently condition the model to propagate these distortions into the synthetic data, potentially exacerbating disparities in downstream decision-making.

Furthermore, this exposes prompt-based adversarial bias injection as a new attack surface. While the tendency of machine learning models to amplify training data biases is well-documented [7, 8, 9], the security implications of in-context bias are underexplored. We introduce a threat model where a malicious actor injects a small number of carefully crafted examples into a collaborative prompt or retrieved context. We demonstrate that this targeted manipulation can skew the synthetic distribution and compromise the fairness of downstream classifiers, all while maintaining high utility metrics that mask the attack.

Contributions. In this paper, we study how in-context examples influence the statistical properties of LLM-generated tabular data. Our contributions are:

- We demonstrate that statistical biases present in ICL examples systematically propagate to the distribution of LLM-generated tabular data, and that LLMs capture and propagate biases in a conditional and intersectional manner. We quantify this propagation via linear sensitivity analysis across multiple model families.
- We introduce a novel perspective on prompt injection, an adversarial setting where a malicious agent *injects* a small number of biased in-context examples into a collaborative data generation pipeline. We show that this targeted manipulation induces fairness violations for the attacked group, demonstrating that an adversary controlling only a small fraction of the prompt can compromise downstream fairness without degrading utility metrics.
- We evaluate in-context pre-processing defenses to mitigate bias injection at the prompt level. We show that in-context defenses consistently reduce statistical parity differences in the synthetic data, and also reduce downstream model disparity with minimal impact on utility in most scenarios. However, we also characterize how bias injection often remains unaddressed for marginal mitigation analysis.

The remainder of this paper is organized as follows. Section 2 reviews related work in tabular generation and fairness. Section 3 details the setup of our adversarial study. Section 4 formalizes and empirically analyses in-context bias propagation. Section 5 studies in-context bias propagation as an adversarial threat. Section 5.2 studies in-context preprocessing techniques as potential mitigation strategies, and Sections 6 and 7 conclude the work.

2. Related Work

Tabular data generation with LLMs. Pretrained language models have emerged as powerful tools for synthesizing tabular data, leveraging broad semantic priors to augment datasets in limited or sensitive domains. These models offer distinct advantages where traditional methods, such as VAEs [2, 10], GANs [11, 2, 3], Diffusion Models [12, 13], and SMOTE [14], struggle to generalize from unrepresentative data [5]. While fine-tuning

approaches like GReaT [1] and Harmonic [15] have demonstrated efficacy in structured data generation, prompting-based methods present a resource-efficient alternative with particular promise for augmenting underrepresented groups. For instance, CuratedLLM [5] utilizes in-context learning (ICL) followed by manual curation to address data scarcity, while Epic [4] relies exclusively on in-context examples and categorical mappings to generate realistic examples. Such capabilities have already been translated to real-world healthcare scenarios to mitigate data scarcity [16]. However, existing prompting methods typically rely on the strong assumption that in-context examples are independent and identically distributed (i.i.d.) with respect to the target distribution. In practice, available data is frequently skewed or demographically imbalanced, and the mechanisms by which these biases propagate during LLM-based tabular generation remain poorly understood.

Fairness in language models. LLMs reproduce and amplify demographic biases inherent in pretraining data, a phenomenon well-studied across benchmarks for both likelihood-based and generative settings [6, 17, 18, 19]. Mitigation strategies mostly rely on decoding and prompting interventions, including self-debiasing [20], fairness-guided prompt search [21], and targeted internal modifications of attention or FFN components [22]. In structured data settings, [23] addresses demographic disparities via in-prompt label manipulations, while [24] improves group fairness in tabular classification through curated exemplars and masking. Recently, [25] studies preprocessing in-context examples to improve fairness in tabular classification. While the mentioned prior works directly use the LLM as a classifier, we investigate fairness in *tabular data generation*, where LLMs are employed to synthetically augment the dataset in scarce scenarios before training a classification downstream model on the generated data if needed.

Beyond unintended bias, we also consider adversarial fairness. While classical fairness attacks typically induce group disparities via training-time data poisoning [26, 27] or backdoors [28], we investigate *prompt fairness attacks* in the generative setting. In our framework, an adversary biases the synthetic distribution not by corrupting the model, but by strategically manipulating in-context exemplars during inference.

3. Experimental setup

Models. We evaluate four open-source LLMs with sizes ranging from 8 billion to 70 billion parameters. These models were selected to represent diverse architectures and sizes, allowing for a study of in-context bias propagation despite varying capabilities stemming from differences in pretraining and alignment. All models are served via vLLM on a cluster of four NVIDIA H100 GPUs. For each experimental setting, we generate 5000 synthetic rows through multiple independent calls, with a batch size of two samples per call.

To preserve statistical independence and mitigate potential ordering biases within the prompt, in-context examples are re-generated and randomized every 10 inference calls. For the

propagation analysis in Section 4, in-context examples are synthetically created, with specific variable biases injected into $\pi \cdot k$ examples (e.g., modifying *race* for univariate bias, or *race* and *target* jointly for conditional bias). On the other hand, for the adversarial study in Section 5, benign examples are drawn i.i.d. from the real dataset, while the remaining $\pi \cdot k$ examples are adversarially manipulated.

Prompts. We adopt the prompt structure from CuratedLLM [5], which decomposes the input into *role*, *task*, and *in-context example* components. We serialize the examples in JSON format and vary the context size $k \in \{20, 40, 60, 80, 100\}$ to simulate realistic data-scarce regimes. The exact prompts are provided in Appendix B.

Datasets. We use the *Adult* [29] and *Compas* [30], *Diabetes*, and *Thyroid* datasets [29], widely used in fairness and healthcare-related research. *Compas* contains recidivism risk assessments, *Adult* includes census income data, *Diabetes* is used for predicting the onset of diabetes based on diagnostic measurements, and *Thyroid* assesses the risk of thyroid disorders based on various clinical and demographic features.

Evaluation Metrics. We evaluate the generated synthetic data across three dimensions: downstream utility, distributional fidelity, and group fairness with respect to a protected attribute. To quantify uncertainty in fairness metrics, we partition the synthetic dataset into 5 blocks and report the mean and standard deviation across them. For downstream fairness (e.g., SPD_D), we train multiple independent models using different seeds and data splits, reporting the mean and standard deviation evaluated on the real test set.

First, to assess utility, we report macro F1 score of each classifier evaluated on the real test set. Second, to measure fidelity (the distributional alignment between real and synthetic data), we employ distinct metrics for categorical and numerical features. For each categorical variable x with support \mathcal{V} , we compute the Total Variation Complement ($1 - TVD$), where TVD is defined as:

$$TVD(\mathcal{D}_R, \mathcal{D}_G) = \frac{1}{2} \sum_{v \in \mathcal{V}} |\mathcal{D}_R(x = v) - \mathcal{D}_G(x = v)|. \quad (1)$$

For numerical variables, we quantify similarity using the Jensen–Shannon divergence (JSD), a smoothed, symmetric version of the Kullback–Leibler divergence:

$$JSD(\mathcal{D}_R \parallel \mathcal{D}_G) = \frac{1}{2} \text{KL}(\mathcal{D}_R \parallel M) + \frac{1}{2} \text{KL}(\mathcal{D}_G \parallel M),$$

where $M = \frac{1}{2}(\mathcal{D}_R + \mathcal{D}_G)$.

Finally, to quantify *fairness*, we measure the Statistical Parity Difference (SPD), which captures the discrepancy in favorable outcomes ($y=1$) between an unprivileged subgroup a_U and a privileged subgroup a_P , for a protected attribute a :

$$SPD = P_{\mathcal{D}_G}(y = 1 | a = a_U) - P_{\mathcal{D}_G}(y = 1 | a = a_P), \quad (2)$$

where for multi-valued protected attributes, we define a_P as the complement of a_U . A value closer to 0 indicates a fairer synthetic distribution that preserves demographic parity. We study both SPD_S of the synthetic data, and SPD_D of the downstream model evaluated on real data. For the downstream model, we also measure Equalized Odds (EOD), defined as the difference between the True Positive Rate and the False Positive Rate of downstream predictions across subgroups:

$$\text{EOD} = \frac{1}{2} (|TPR_{a_U} - TPR_{a_P}| + |FPR_{a_U} - FPR_{a_P}|), \quad (3)$$

and Equal Opportunity (EO), defined as the absolute difference in True Positive Rates (TPR) between subgroups:

$$\text{EO} = |TPR_{a_U} - TPR_{a_P}|, \quad (4)$$

where $TPR_a = P(\hat{y} = 1 | y = 1, a)$ denotes the True Positive Rate for the downstream model predictions $\hat{y} = 1$, and $FPR_a = P(\hat{y} = 1 | y = 0, a)$ denotes the False Positive Rate for a subgroup a and unfavorable outcome $y = 0$.

4. In-Context Bias Propagation in LLM-generated Data

Given a supervised classification task, a downstream model learns a function $f \in \mathcal{F}$, $f : \mathcal{X} \rightarrow \mathcal{Y}$, where \mathcal{X} is the feature space, and \mathcal{Y} is the label space. We assume an underlying distribution \mathcal{D} over triples $(x, a, y) \in \mathcal{X} \times \mathcal{A} \times \mathcal{Y}$, where a is the protected attribute, and an observed labeled dataset $S_{\text{train}} = \{(x_i, a_i, y_i)\}_{i=1}^n$ with $(x_i, a_i, y_i) \stackrel{\text{i.i.d.}}{\sim} \mathcal{D}$. In data scarce scenarios, where $n < 100$, the prior knowledge of pretrained language models has been shown to be a resource efficient alternative for synthetic data augmentation [5], improving utility of the downstream classifier.

Let M be a pretrained language model. The LLM-based tabular data augmentation process is guided by a prompt P containing k serialized demonstration examples $\{x_1, \dots, x_k\}$ drawn i.i.d. from S_{train} . We define \mathcal{D}_G as the generated distribution, i.e., the distribution of synthetic examples produced by M when queried with k in-context examples. We also define $\tilde{\mathcal{D}}_0$ as an anchor prior distribution, obtained as the distribution of examples generated by M using the same prompt template but with $k = 0$ in-context examples. This distribution captures the model’s internal prior for the given task.

To quantify bias π , which is the ratio of adversarial examples within the prompt, we consider a bounded statistic $\phi : \mathcal{X} \times \mathcal{A} \times \mathcal{Y} \rightarrow \mathbb{R}$. For a probability distribution \mathcal{D} , the associated scalar bias is $\mu_\phi(\mathcal{D}) = \mathbb{E}_{z \sim \mathcal{D}}[\phi(z)]$. Our goal is to relate π to the bias shift $|\mu_\phi(\mathcal{D}_G) - \mu_\phi(\tilde{\mathcal{D}}_0)|$ observed between the reference distribution $\tilde{\mathcal{D}}_0$ and the ICL-generated distribution \mathcal{D}_G .

4.1. Modeling In-Context Sensitivity

Recent work interprets in-context learning as approximate Bayesian inference [31, 32], where pretraining induces a prior over latent tasks and the prompt provides evidence that shifts the model’s predictions. In this view, the resulting predictive distribution behaves like a mixture of task-conditional predictors,

with weights that depend on the prompt. Motivated by this perspective, we use the following two-component decomposition to study in-context influence on tabular synthesis

$$\mathcal{D}_G \approx (1 - \alpha_k) \tilde{\mathcal{D}}_0 + \alpha_k \Phi_M(\mathcal{D}_P), \quad (5)$$

where $\tilde{\mathcal{D}}_0$ is a zero-shot anchor distribution induced by pretraining (same template, $k = 0$), $\Phi_M : \mathcal{P}(\mathcal{X}) \rightarrow \mathcal{P}(\mathcal{X})$ denotes the model-dependent transformation from an empirical prompt distribution to the corresponding k -shot generation distribution, and $\alpha_k \in [0, 1]$ summarizes the overall strength of prompt conditioning at context size k .

For $k > 0$, prompting artifacts (serialization, length) can induce distribution shifts even when demonstrations are unbiased. To control for this, we define the reference distribution $\mathcal{D}_0 := \Phi_M(\tilde{\mathcal{D}}_0)$, obtained by prompting the model with k examples drawn from the zero-shot anchor $\tilde{\mathcal{D}}_0$ rather than the training data. We quantify the propagation of statistical skews using a drift score $D_f(\cdot, \cdot)$. We measure prompt drift as $D_f(\mathcal{D}_P, \mathcal{D}_0)$ and the resulting generation drift as $D_f(\mathcal{D}_G, \mathcal{D}_0)$. We empirically study whether controlled perturbations of \mathcal{D}_P induce linear changes in $D_f(\mathcal{D}_G, \mathcal{D}_0)$.

Finally, we connect distributional drift directly to our fairness objective. Since fairness metrics are derived from the underlying data distribution, the score $D_f(\mathcal{D}_G, \mathcal{D}_0)$ effectively drives the induced bias shift $|\mu_\phi(\mathcal{D}_G) - \mu_\phi(\mathcal{D}_0)|$. In the following section, we therefore focus on characterizing how demographic skews in the in-context examples affect statistical parity in both the synthetic output and downstream classifiers.

4.2. Experimental Results

In this section, we systematically quantify the sensitivity of LLM-based tabular generation to statistical distortions within in-context examples. We structure our analysis across three levels of granularity: (i) marginal bias propagation, examining univariate shifts in protected attributes; (ii) conditional bias propagation, focusing on induced correlations between protected groups and target labels; and (iii) intersectional propagation, which evaluates bias amplification across joint subgroups. By varying the bias intensity (π) and number of in-context examples (k) across multiple model families, we characterize the dynamics of this bias propagation, establishing the empirical foundation for the adversarial vulnerabilities discussed in Section 5.

4.2.1. Experimental setup

In our Section 4 experiments, we use two prompt structures. (i) First, we use the *unconstrained* prompt for marginal bias propagation analysis, which does not include any extra instructions. (ii) Second, for our conditional and intersectional bias propagation analysis, we use the *balanced* prompt; this explicitly instructs the LLM to generate one example per subgroup with the goal of keeping frequency counts approximately balanced in \mathcal{D}_G , thus isolating conditional bias from subgroup frequency imbalances. Both prompts incorporate k in-context demonstrations serialized in JSON format and drawn from a biased distribution \mathcal{D}_P . We measure marginal propagation strength using a drift score D_f , defined as the sum of the mean TVD for categorical

variables and the mean JSD for numerical variables. In-context examples are drawn from \mathcal{D}_0 , and for each analysis, we modify the probability of the studied variable.

4.2.2. Marginal Bias Propagation

We begin by quantifying the sensitivity of LLM-generated distributions (\mathcal{D}_G) to univariate statistical distortions within the $k \in \{20, 40, 60, 80\}$ in-context examples drawn from \mathcal{D}_P . We focus specifically on the propagation of imbalances in protected attributes, such as race or gender. In this regard, Figure 2 presents the analysis for *Mixtral-8x7b* under varying levels of racial bias intensity π , defined as the fraction of in-context examples assigned to a specific target group (e.g., *Black*), while remaining attributes are sampled from the anchor distribution \mathcal{D}_0 .

In Figure 2 (left), we compare the divergence of the prompt distribution, $D_f(\mathcal{D}_P, \mathcal{D}_0)$, against the resulting divergence in the generated distribution, $D_f(\mathcal{D}_G, \mathcal{D}_0)$. Given the no-ICL (zero-shot) model’s prior distribution $\tilde{\mathcal{D}}$, we construct $\mathcal{D}_0 = \phi_M(\tilde{\mathcal{D}})$ as the reference distribution. We observe a linear relationship between the input and output distributional shifts, with increases in π producing proportional increases in the divergence of \mathcal{D}_G . Moreover, Figure 2 (right) demonstrates that the resulting probability of the target racial group in the synthetic output scales linearly with the underlying probability in the prompt.

Figure 2 (bottom) replicates the analysis for gender bias, with target group Female. While the linear sensitivity persists, the distributional drift for gender is attenuated compared to race. This discrepancy suggests a non-trivial interaction between the model’s pre-trained priors and the in-context evidence with respect to \mathcal{D}_0 . However, the target gender probability retains a strictly linear relationship with π , confirming that the propagation mechanism remains consistent even when the distributional shift with respect to \mathcal{D}_0 varies.

The remainder of this section systematically characterizes this propagation behavior across three dimensions: prompt composition, context size, and model architecture. Our findings reveal that even mild perturbations in \mathcal{D}_P can systematically skew the statistical parity of synthetic data, introducing significant fairness risks in tabular generation pipelines.

Number of in-context examples. We argue that the context size k directly modulates the bias propagation strength, modeled as α_k in Equation 5. As k increases, the synthetic distribution \mathcal{D}_G diverges from the model’s intrinsic zero-shot prior and increasingly aligns with the empirical prompt distribution \mathcal{D}_P .

In Figure 3 (left), we validate this effect for a fixed $k = 80$ across all four model families. We observe that the probability of the synthetic samples belonging to the targeted Black subgroup scales approximately linearly with the bias intensity π injected into the in-context examples. Specifically, at $\pi = 0$, the output distribution remains close to the anchor baseline ($p_{\mathcal{D}_0}(\text{Race} = \text{Black})$), but as π increases, the LLMs exhibit consistent sensitivity to the univariate racial skews present in the prompt. Notably, different models exhibit varying degrees of sensitivity to the same prompt biases, with some models showing stronger alignment with the prompt distribution than others.

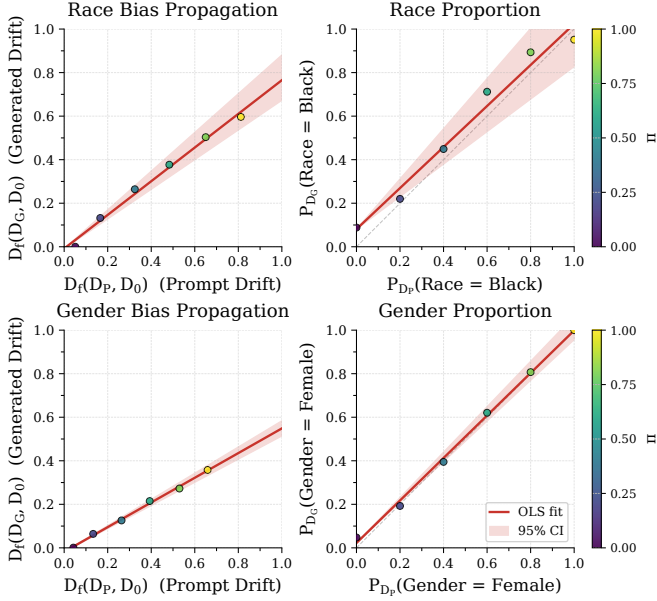


Figure 2: **Marginal in-context bias propagation** (*Mixtral-8x7b*, $k = 80$). (Left) Drift in the generated distribution $D_f(\mathcal{D}_G, \mathcal{D}_0)$ versus drift in the prompt distribution $D_f(\mathcal{D}_P, \mathcal{D}_0)$. The linear relationship shows that distributional shifts in prompts are proportionally transferred to synthetic outputs. (Right) Probability of the target group (Race/Gender) in generated samples increases linearly with prompt bias intensity π , confirming that LLMs propagate univariate demographic skews from in-context examples.

To quantify this sensitivity across different context sizes, we compute the propagation coefficient β_k by fitting an ordinary least squares (OLS) regression between the drift of the prompt distribution from the anchor, $D_f(\mathcal{D}_P, \mathcal{D}_0)$, and the drift of the generated distribution from the anchor, $D_f(\mathcal{D}_G, \mathcal{D}_0)$. Figure 3 (right) demonstrates that β_k increases monotonically with k across all models, indicating that larger context windows amplify the propagation of distributional shifts from prompts to synthetic outputs. While both β_k and the absolute magnitude of distributional shifts vary significantly between architectures (see Appendix A), the fundamental linear relationship between the probability of synthetic examples from a targeted group and their proportion in the in-context examples remains consistent across all model families.

These findings are consistent with the mechanism underlying prior observations that larger context windows improve synthetic data fidelity [4, 24]. When \mathcal{D}_P represents the ground truth ($\mathcal{D}_P \equiv \mathcal{D}_R$), a large k ensures high utility by aligning the output with real-world statistics. However, our results in Figures 3 and 4 demonstrate that this same mechanism creates a critical vulnerability, as when \mathcal{D}_P is demographically skewed, larger k values faithfully replicate and amplify these distortions into the synthetic dataset.

4.2.3. Conditional Bias Propagation

While the previous univariate propagation analysis demonstrates that LLMs faithfully replicate marginal distributions within in-context examples, real-world biases often manifest through complex correlations between protected attributes and

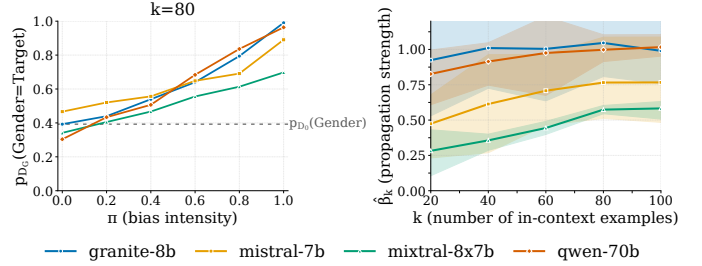


Figure 3: **Marginal bias propagation across model families.** (Left) Probability of the target group in generated samples increases linearly with prompt bias intensity π for all models at $k = 80$. The dashed line shows the anchor baseline $p_{\mathcal{D}_0}(\text{Target})$. (Right) Propagation coefficient β_k increases monotonically with context size k across all models.

outcome variables. To investigate this, we now examine how LLMs learn and reproduce statistical correlations between a protected subgroup (e.g., a specific gender) and a target label (e.g., high income) from biased in-context examples.

We induce targeted conditional bias by constructing prompts where examples from a protected subgroup $\mathcal{S}_{\text{target}}$ (e.g., Female) are systematically correlated with a positive outcome $Y = 1$ (e.g., High Income). To disentangle conditional dependence from frequency effects, we explicitly instruct the LLM to generate a balanced number of examples across subgroups with the *balanced prompt* defined in Section 4.2.1. We vary the bias intensity π , defined as the positive label probability for the target group $\mathcal{S}_{\text{target}}$ in-context examples, while maintaining a constant positive label probability of 0.5 for the non-targeted subgroup.

As shown in Figure 5, *Mixtral-8x7b* effectively captures the conditional probability $P(Y = 1 | \mathcal{S}_{\text{target}})$ from the in-context examples and propagates it to synthetic examples. The left figure demonstrates that as π increases, the probability of generating high-income examples for the targeted Female subgroup increases proportionally, while the non-targeted Male subgroup remains stable near 0.5. Furthermore, comparing curves at $k = 20$ versus $k = 80$ reveals that the generated conditional distribution aligns more closely with prompt statistics at larger context sizes. This increased fidelity is quantified in Figure 5 (right) through the statistical parity difference (SPD) between subgroups, which shows a steeper increase with π at $k = 80$ compared to $k = 20$. These findings illustrate how conditional bias propagation affects fairness metrics even when univariate marginals are balanced, and demonstrate that larger in-context windows amplify the model’s sensitivity to conditional correlations in the prompt.

Model-specific behavior. Figure 6 summarizes model-specific sensitivity to injected conditional bias by reporting the slope of the linear fit between bias intensity π and the predicted positive rate for each gender subgroup. Across all models, the targeted subgroup (*Female*) exhibits substantially steeper slopes than the non-targeted subgroup (*Male*), confirming that the injected correlation is consistently learned in a group-specific manner. The non-targeted subgroup shows minimal growth, indicating limited spillover of the injected bias. Within the same family (*Mistral-7B* vs. *Mixtral-8x7B*), the mixture-of-experts model displays stronger conditional propagation, consistent with the

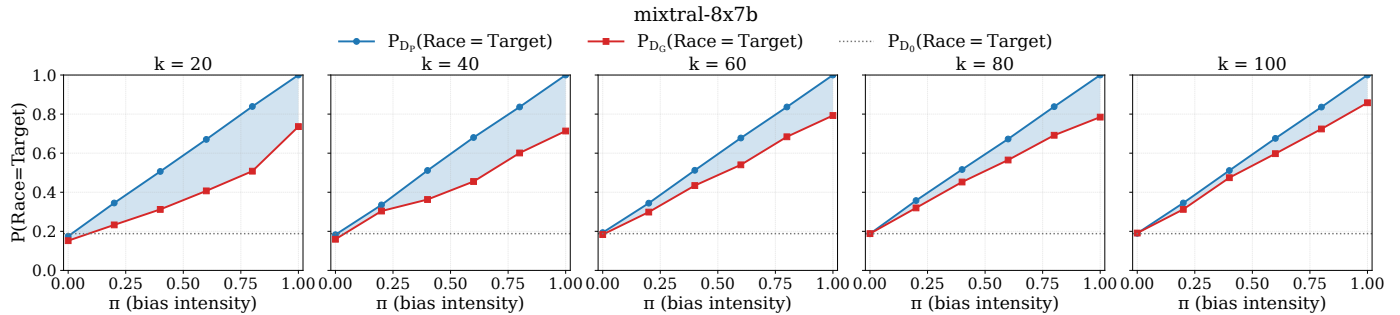


Figure 4: **Bias propagation strength increases with context size.** Each subfigure shows results for a different context size $k \in \{20, 40, 60, 80\}$. The red curve shows the target group probability in generated samples $p_{D_C}(\text{Target})$, the blue curve shows the target group probability in prompt examples $p_{D_P}(\text{Target})$, and the dashed line shows anchor baseline $p_{D_0}(\text{Target})$. As k increases, the red curve converges toward the blue curve, indicating that larger context windows lead to stronger replication of prompt-level demographic distributions.

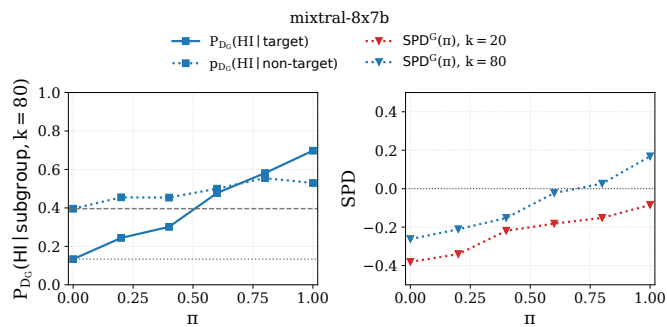


Figure 5: **Conditional bias propagation for targeted and non-targeted subgroups.** (Left) Conditional probability of generating High Income examples for each gender subgroup as the bias intensity π increases. The targeted subgroup exhibits strong linear sensitivity to π , while the non-targeted subgroup remains near 0.5. (Right) Statistical parity difference (SPD) between subgroups increases more steeply at $k = 80$ than $k = 20$, demonstrating that larger context windows amplify conditional bias propagation.

hypothesis that increased model capacity enables better capture of complex conditional dependencies within the prompt. Similarly, Qwen-70B achieves the highest propagation slopes among all evaluated models, suggesting that both model scale and architecture influence the strength of conditional bias transfer.

4.2.4. Intersectional Bias Propagation

Next, we study whether LLMs propagate intersectional patterns that emerge only at the joint level of multiple protected attributes, beyond what univariate or conditional analyses can capture. We focus on the Adult dataset and consider the four intersectional groups defined by gender $\in \{\text{Male}, \text{Female}\}$ and race $\in \{\text{Black}, \text{White}\}$. For a fixed context size k , we construct an *intersectional* prompt ensuring balanced frequency counts across all four groups, such that the marginal distributions over gender and race remain approximately uniform. We configure the LLM to generate one example from each subgroup per call using the *balanced prompt* defined in Section 4.2.1. We then manipulate the high-income target probability using $\pi \in [0, 1]$, simultaneously increasing the positive rate for $\{\text{Female}, \text{Black}\}$ and $\{\text{Male}, \text{White}\}$ while decreasing it for $\{\text{Female}, \text{White}\}$ and $\{\text{Male}, \text{Black}\}$. This design creates a bias pattern that cannot be

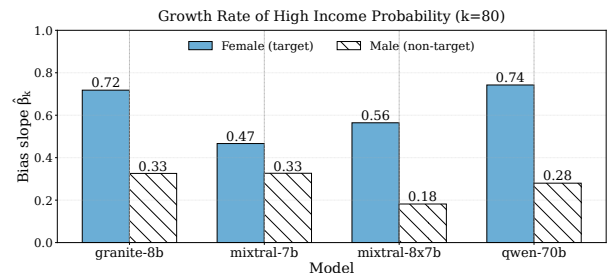


Figure 6: **Model-specific sensitivity to conditional bias propagation.** ($k=80$, Adult) The slope β_k quantifies how strongly the predicted positive rate for each gender subgroup changes with bias intensity π . We estimate β_k by fitting a linear regression to $P(Y = 1 | \text{subgroup})$ across values of π . All models show substantially steeper slopes for the targeted (*Female*) subgroup compared to the non-targeted (*Male*) subgroup, indicating systematic propagation of the injected correlation. The magnitude varies across architectures, with larger and mixture models exhibiting stronger conditional bias transfer.

detected by examining gender or race in isolation compared to the original biases in $\pi = 0.0$.

Figure 7 reports the positive label probabilities for Granite-8b on Adult across different context sizes. Each subfigure corresponds to a different value of k , and each curve tracks one intersectional group as π increases. The LLM reliably reproduces the injected pattern: $\{\text{Female}, \text{Black}\}$ and $\{\text{Male}, \text{White}\}$ exhibit monotonic increases in $P(Y=1)$ with π , while $\{\text{Female}, \text{White}\}$ and $\{\text{Male}, \text{Black}\}$ either plateau or decrease. The separation between targeted and non-targeted subgroups widens at higher k , indicating that intersectional propagation strength grows with the number of in-context examples.

Figure 8 provides a complementary visualization through heatmaps of high-income probabilities across the four intersectional cells. At $\pi = 0$ (left), all four cells exhibit similar probabilities around 0.3-0.5, reflecting the model’s intrinsic biases. At $\pi = 0.6$ (right), probability mass moves to the targeted $\{\text{Female}, \text{Black}\}$ and $\{\text{Male}, \text{White}\}$ cells (dark red), while non-targeted subgroups show lower probabilities. This bias pattern induced by the intersectional bias now influences the baseline marginal disparities present at $\pi = 0$. While LLMs carry inherent group-level biases from pretraining, they simultaneously amplify intersectional correlations injected through in-context examples, creating compound discrimination patterns where

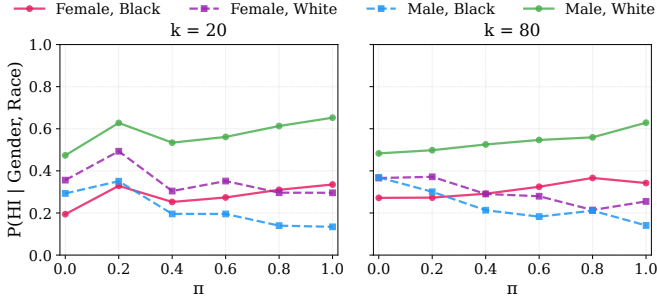


Figure 7: **Multivariate intersectional probabilities.** (*Granite-8b*) Conditional probability of high income for each gender–race cell in the generated data as a function of the intersectional bias strength π , for different context sizes k . As π and k increase, the LLM amplifies the intersectional pattern injected in the prompt.

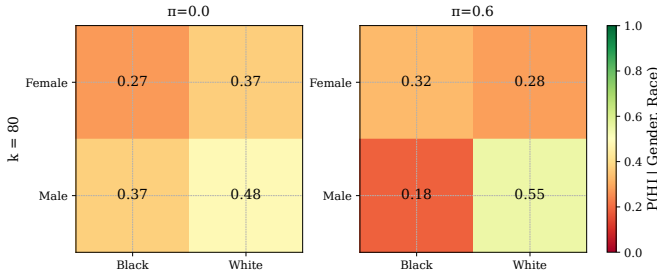


Figure 8: **Intersectional high-income probability heatmap.** (*Granite-8b*) Conditional probability of high income $P(\text{HI} | \text{gender, race})$ in the generated data for Adult under the intersectional bias. The left figure corresponds to an unbiased prompt ($\pi = 0$), generated with in-context examples drawn from D_0 , while the right panel shows a fully biased prompt ($\pi = 0.6$) in which (Female, Black) and (Male, White) are high-income cells. The model amplifies this injected intersectional pattern, raising $P(\text{HI})$ for the high income subgroups and lowering it for the other subgroups.

both sources of bias interact.

5. Adversarial In-Context Bias Injection

In the previous section, we analyzed in-context bias propagation as a potential *risk* that might appear in LLM-based synthetic tabular data generation, arising from imbalances in the available data. In this section, we adopt a security perspective and investigate whether a malicious user can craft a small number of in-context examples that deliberately manipulate the statistical properties of the synthetic data for a targeted subgroup, without altering downstream model performance.

Threat Model. We consider a collaborative data generation pipeline in which multiple users independently contribute few-shot in-context examples to a shared LLM service. This scenario can also be viewed as populating a database, which is sampled to generate in-context examples through a RAG-service. Here, a malicious user could further leverage RAG vulnerabilities [33] to influence the selection of examples that are adversarially injected. These examples are added into the prompt, which is then forwarded to the LLM to generate synthetic tabular data. An adversary is able to control a fraction π of the k examples in the

prompt, but does not have access to the model parameters or to the in-context examples provided by honest users. We assume that the attacker knows (i) the protected attribute (e.g., race or gender), (ii) the downstream prediction task and the target label, and (iii) general domain knowledge regarding the dataset attributes. The adversary’s objective is to influence the label rate of a protected group in the synthetic data (e.g., the proportion of high-income labels assigned to Black individuals in the Adult dataset), while preserving high overall utility.

Table 1: Attributes used to construct adversarial feature-aligned examples for each dataset.

Dataset	Protected Attr	Target Label	Feature-Aligned Values
Compas	Race: African-American	Recidivism (1)	Priors: 3–8 Age: 18–45 Juv. Felonies: 0 Charge Degree: M or F (Random)
Adult	Gender: Female Marital-status: Married-civ-spouse Native-country: United-States	Income: >50K	Age: 30–55 Education: HS-grad or Some-college Hours/Week: 38–41 Capital Loss: 0–50
Diabetes	Age: 21–30	Diabetes (1)	Glucose: 120–155 BMI: 27.0–33.0 Insulin: 80–180 Pedigree: 0.6–1.2
Thyroid	Age: 20–35	High Risk (2)	Goiter: 0 or 1 (Random) Family History: 0 or 1 (Random) Fatigue: 0 or 1 (Random) Gender: 0 (Female)

In this regard, the adversary constructs *feature-aligned* examples, i.e., examples designed to embed strong correlations between the protected group and the target label, while maintaining plausible values for non-targeted attributes. Leveraging domain knowledge, these plausible values (see Table 1) are set to simulate moderate risk profiles (e.g., 3-8 priors for Compas, standard working hours for Adult) rather than extreme outliers. This strategy ensures the examples remain statistically realistic to evade outlier detection while efficiently driving the biased correlation. Following the bias propagation analysis from Section 4, increasing the target label probability for a targeted subgroup will propagate to the synthetic data, which in turn might influence the downstream model to rely on the targeted attribute for a biased prediction, even when the attribute itself is originally ignored as predictive feature by the downstream model.

Experimental setup. Let k denote the total number of in-context examples. An adversary controls a fraction $\pi \in [0, 1]$ of these examples and injects πk malicious, feature-aligned records into the prompt, while the remaining $(1 - \pi)k$ examples are sampled i.i.d. from the real dataset. We use a pre-trained LLM to augment from 80 available samples to a synthetic tabular dataset of 5000 rows. As non-LLM baselines, we include for comparison classical synthetic tabular data generators (TVAE, CTGAN, NFLOW, DDPM), also generating synthetic data from $k = 80$ real examples.

Table 1 summarizes, for each dataset, the protected attribute, the target label, and the feature-aligned attributes that the attacker manipulates. For Adult and Compas, the protected attribute is categorical, while for Diabetes and Thyroid, it is numerical (Age). For Adult, we define the protected subgroup as

the intersection of (gender, native-country, marital-status) values to study intersectional bias propagation. We use Adult, Compas, and Diabetes datasets for binary classification tasks, and Thyroid for a multi-class classification task.

For each synthetic dataset produced under a given (π, k) configuration and LLM, we train downstream classifiers –Random Forest, Gradient Boosting, Logistic Regression, and the LLM-based TabPFN –on the synthetic training split and evaluate them on the real test set. We report in Table 2 the Macro F1 score as utility metric and the statistical parity difference (SPD) as fairness metric for both the synthetic data (SPD_S) and the downstream model (SPD_D). Together with the distributional fidelity metrics in Table 3, these results allow us to study how targeted in-context biases affect both the quality and the fairness of LLM-generated tabular data.

5.1. Experimental Results

Feature-aligned examples. For recidivism prediction on Compas, attributes such as the number of prior convictions, juvenile felonies, and the charge degree are among the strongest predictors used by the downstream classifier. In our adversarial setting, the attacker uses common domain knowledge to create *feature-aligned* in-context examples for the protected subgroup by setting these attributes to plausible values. For instance, an adversarial example for the Compas task would correspond to an African-American (AA) individual who commits recidivism, has a small prior-count (e.g., 5), no juvenile felonies, and a low-severity (misdemeanor) charge degree. When such records are injected as a fraction π of the in-context demonstrations, the LLM is influenced to generate synthetic data in which protected-group individuals that induce the correlation $p(y = 1|race = AA)$ have plausible values for non-protected attributes. This, in turn, might induce downstream classifiers trained on the synthetic data to rely on the protected attribute (i.e., race) for recidivism predictions, even when the group attribute is not explicitly intended as a predictive feature. The effect of feature-aligned examples in the synthetic data is illustrated in Figure A.17, where as π increases, the normalized density of key Compas predictors for the protected subgroup (African-American) shifts toward the adversarially set feature values, while the complementary group remains closer to the original distribution.

Before the complete analysis on adversarial bias propagation, we examine how variations in the targeted adversarial attribute within in-context examples affect downstream performance. To do so, we train a Random Forest classifier on each synthetic dataset under (i) race-aware, where the protected attribute is included in the downstream decision, and (ii) race-blind scenarios, where the protected attribute is excluded. This comparison shows whether the correlations inherent in feature-aligned examples are successfully propagated to the synthetic data and subsequently learned by the downstream model.

In this regard, Figure 10 reports the resulting downstream SPD together with race feature importance, measured via Mean Decrease Impurity (MDI) –a metric quantifying the feature’s contribution to reducing uncertainty in the Random Forest’s decision splits. As π increases, downstream disparity increases notably in the race-aware setting with a corresponding increase

in race influence on downstream predictions, indicating that the injected correlation between the targeted racial group and the label causes the downstream model to increasingly rely on the race attribute for prediction. Removing race from the prediction variables attenuates the race disparity between protected groups but still shows a minor increase with π , which indicates that the downstream model potentially captures correlations between aligned features and the target variable even when the protected variable is not present.

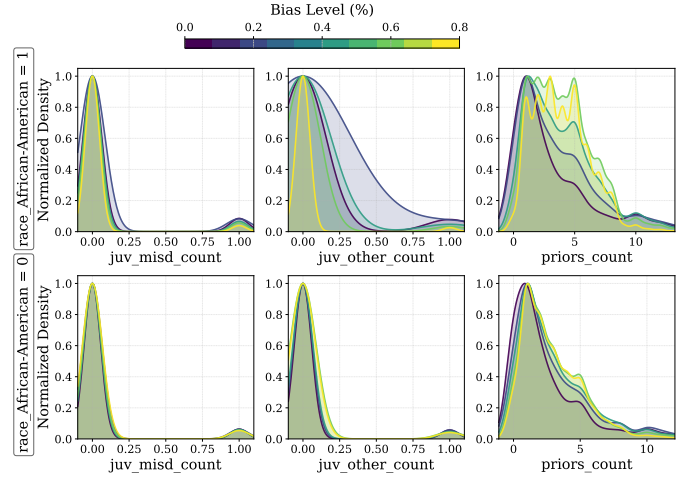


Figure 9: **Normalized density of aligned features.** (Mixtral-8×7B, $k=80$ ICL examples, Compas) Synthetic univariate distributions of key recidivism predictors for the protected subgroup (African-American) and the complementary group, as the fraction of biased in-context examples π increases. The attack steers African-American records towards the plausible values set by the attacker (e.g., low prior counts and fewer juvenile offenses) while leaving the non-targeted group closer to the baseline, illustrating how a number of adversarial examples can selectively reshape the synthetic feature profile of a protected subgroup.

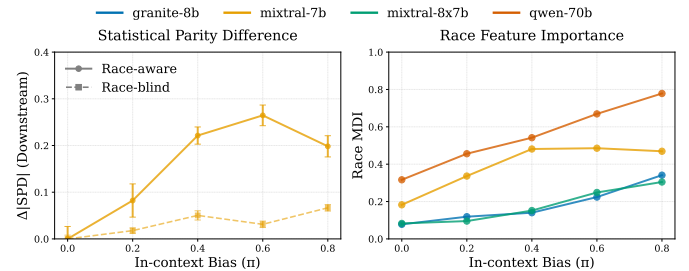


Figure 10: **Downstream fairness and race importance vs in-context bias π .** (Left) $\Delta|SPD|$ of downstream model predictions on the real dataset when fitted on the synthetic dataset, including and excluding race features. (Right) Race feature MDI importance in the Random Forest classifier trained on synthetic data generated with various LLMs.

Fairness impact on synthetic data. Table 2 shows that even moderate attack rates ($\pi = 0.3$) induce substantial group disparities (SPD_S) in the synthetic datasets across all models and datasets. For Compas, increasing the bias rate from $\pi = 0$ to $\pi = 0.3$ moves SPD_S from -0.13 to -0.25 for Granite-8B, and from -0.14 to -0.25 for Qwen-70B, nearly doubling the imbalance in both cases. Similar trends appear in Adult, Diabetes, and

Table 2: Utility and fairness metrics (F1-Score, SPD) across four datasets ($k=80$). For each dataset, we train the Random Forest downstream classifier with the synthetic dataset, and report F1 score on the real dataset ($F1_R$), SPD on the synthetic data (SPD_S), and SPD of the downstream model (SPD_D).

Model	π	Adult			Compas			Diabetes			Thyroid		
		$F1_R \uparrow$	$SPD_S \downarrow$	$SPD_D \downarrow$	$F1_R \uparrow$	$SPD_S \downarrow$	$SPD_D \downarrow$	$F1_R \uparrow$	$SPD_S \downarrow$	$SPD_D \downarrow$	$F1_R \uparrow$	$SPD_S \downarrow$	$SPD_D \downarrow$
Real oracle	–	0.85	–	0.13 _{0.00}	0.62	–	-0.13 _{0.00}	0.73	–	0.29 _{0.00}	0.86	–	-0.06 _{0.00}
TVAE	0.0	0.45	-0.04 _{0.00}	-0.04 _{0.00}	0.53	-0.04 _{0.00}	0.01 _{0.00}	0.66	-0.04 _{0.00}	0.06 _{0.00}	0.49	-0.04 _{0.00}	-0.11 _{0.00}
CTGAN	0.0	0.51	0.78 _{0.00}	0.07 _{0.00}	0.58	0.52 _{0.00}	-0.04 _{0.00}	0.67	0.74 _{0.00}	0.42 _{0.00}	0.46	0.56 _{0.00}	-0.13 _{0.00}
NFLOW	0.0	0.57	0.51 _{0.00}	0.10 _{0.00}	0.57	0.64 _{0.00}	-0.03 _{0.00}	0.50	0.51 _{0.00}	0.02 _{0.00}	0.44	0.44 _{0.00}	0.02 _{0.00}
DDPM	0.0	0.51	0.01 _{0.02}	0.01 _{0.02}	0.52	-0.62 _{0.01}	-0.17 _{0.07}	0.39	0.09 _{0.02}	-0.01 _{0.01}	0.58	0.37 _{0.04}	-0.04 _{0.01}
Granite-8B	0.0	0.74	-0.17 _{0.14}	-0.10 _{0.02}	0.59	-0.13 _{0.02}	-0.12 _{0.02}	0.72	0.21 _{0.05}	0.32 _{0.01}	0.54	0.22 _{0.07}	0.06 _{0.02}
	0.3	0.73	-0.50 _{0.04}	-0.21 _{0.02}	0.56	-0.25 _{0.02}	-0.32 _{0.01}	0.77	0.09 _{0.00}	0.26 _{0.01}	0.48	-0.20 _{0.04}	-0.13 _{0.01}
	0.6	0.75	-0.59 _{0.02}	-0.28 _{0.02}	0.57	-0.33 _{0.02}	-0.29 _{0.01}	0.73	-0.03 _{0.01}	0.24 _{0.01}	0.44	-0.27 _{0.01}	-0.14 _{0.01}
Mistral-7B	0.0	0.64	0.15 _{0.01}	-0.03 _{0.01}	0.52	-0.19 _{0.01}	-0.05 _{0.01}	0.71	0.25 _{0.03}	0.19 _{0.01}	0.44	0.44 _{0.00}	0.07 _{0.00}
	0.3	0.66	-0.18 _{0.07}	-0.13 _{0.02}	0.49	-0.38 _{0.01}	-0.27 _{0.02}	0.69	0.12 _{0.01}	0.13 _{0.01}	0.45	0.06 _{0.04}	-0.10 _{0.02}
	0.6	0.65	-0.23 _{0.01}	-0.15 _{0.02}	0.55	-0.43 _{0.01}	-0.35 _{0.02}	0.68	-0.02 _{0.00}	0.09 _{0.01}	0.37	-0.08 _{0.03}	-0.09 _{0.01}
Mixtral-8x7B	0.0	0.72	-0.17 _{0.02}	-0.16 _{0.02}	0.54	-0.14 _{0.01}	-0.23 _{0.01}	0.73	0.33 _{0.04}	0.27 _{0.01}	0.53	0.14 _{0.06}	-0.03 _{0.01}
	0.3	0.71	-0.28 _{0.02}	-0.20 _{0.02}	0.53	-0.25 _{0.01}	-0.27 _{0.01}	0.79	0.20 _{0.01}	0.22 _{0.01}	0.55	-0.09 _{0.00}	-0.15 _{0.00}
	0.6	0.67	-0.33 _{0.01}	-0.14 _{0.02}	0.53	-0.41 _{0.03}	-0.43 _{0.01}	0.76	0.12 _{0.00}	0.20 _{0.01}	0.49	-0.11 _{0.01}	-0.13 _{0.00}
Qwen-70B	0.0	0.73	-0.11 _{0.02}	-0.09 _{0.02}	0.56	-0.51 _{0.04}	-0.34 _{0.02}	0.69	0.70 _{0.02}	0.37 _{0.01}	0.57	0.39 _{0.01}	0.08 _{0.01}
	0.3	0.73	-0.35 _{0.04}	-0.15 _{0.02}	0.56	-0.72 _{0.01}	-0.43 _{0.02}	0.73	0.51 _{0.03}	0.29 _{0.01}	0.57	0.07 _{0.04}	-0.02 _{0.02}
	0.6	0.72	-0.36 _{0.00}	-0.11 _{0.01}	0.56	-0.85 _{0.02}	-0.57 _{0.02}	0.72	0.20 _{0.02}	0.19 _{0.01}	0.57	-0.21 _{0.01}	-0.08 _{0.00}

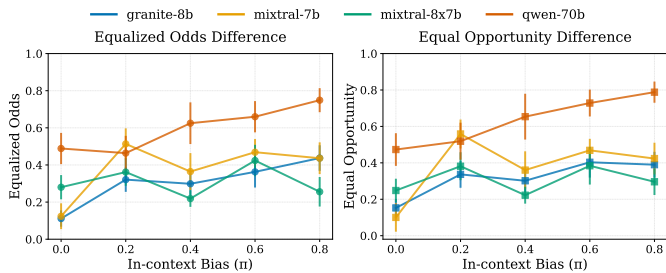


Figure 11: (Granite-8b, Compas). Equalized odds (left) and equal opportunity (right) of downstream model predictions on the real dataset across data generated with various LLMs and in-context bias π .

Thyroid, where for the more vulnerable models, SPD_S typically increases by 0.2–0.3 between $\pi = 0$ and $\pi = 0.6$. Notably, at $\pi = 0.3$, the shift already exceeds 0.1, a threshold established by Baracaldo et al. [34] as a criterion for a successful fairness attack. These shifts occur despite the adversary only controlling a fraction of the demonstrations, confirming that LLM-based tabular generators are sensitive to in-context manipulation along fairness dimensions.

Distributional fidelity. The fidelity metrics in Table 3 demonstrate a monotonic degradation in marginal distributional similarity to the real data as the adversarial bias rate π increases, with Jensen–Shannon Divergence (JSD) exhibiting significant drift (e.g., rising from 0.258 to 0.405 for Qwen-70B on Compas). While this confirms that feature-aligned injections distort synthetic data, we argue this degradation remains stealthy, as the very premise of few-shot augmentation ($k = 80$) implies the absence of a large, representative reference distribution against which to benchmark metrics like JSD in practice. Consequently, without access to ground-truth data for validation, even substantial deviations in global statistics are likely to pass undetected with marginal analyses, underscoring how standard dataset-level

Table 3: Fidelity of the synthetic dataset to the real dataset for different models and bias rates. We show Jensen–Shannon Divergence (JSD) for numerical variables and Total Variation (TV) for categorical variables. The Diabetes dataset has only numerical features, so we report only JSD.

Model	π	Adult		Compas		Diabetes	Thyroid	
		JSD \downarrow	TVC \uparrow	JSD \downarrow	TVC \uparrow	JSD \downarrow	JSD \downarrow	TVC \uparrow
Granite-8B	0.0	0.096	0.790	0.258	0.895	0.340	0.183	0.971
	0.3	0.122	0.754	0.366	0.890	0.342	0.221	0.911
	0.6	0.201	0.724	0.484	0.824	0.377	0.269	0.819
Mistral-7B	0.0	0.161	0.716	0.318	0.871	0.263	0.232	0.927
	0.3	0.186	0.622	0.411	0.905	0.297	0.242	0.873
	0.6	0.242	0.577	0.488	0.904	0.334	0.249	0.816
Mixtral-8x7B	0.0	0.115	0.767	0.230	0.906	0.264	0.175	0.917
	0.3	0.147	0.753	0.323	0.898	0.272	0.237	0.824
	0.6	0.203	0.720	0.418	0.892	0.310	0.317	0.733
Qwen-70B	0.0	0.174	0.768	0.258	0.813	0.703	0.331	0.915
	0.3	0.174	0.729	0.335	0.836	0.370	0.358	0.811
	0.6	0.232	0.693	0.405	0.892	0.751	0.385	0.743

diagnostics fail to expose group-specific bias manipulations in data-scarce regimes where LLM augmentation is most valuable.

Propagation to downstream models. Here, we study how the adversarial biases injected into the synthetic data propagate to the downstream model. Figure 12 summarizes the behavior of the downstream Random Forest classifier on Compas as a function of the in-context bias rate π . While the macro F1 on real data (blue curves) remains nearly flat across all levels of π , the absolute SPD of the downstream predictions (grey curves) increases monotonically for several models. For Mistral-7B, SPD_D grows from -0.05 at $\pi = 0$ to -0.35 at $\pi = 0.6$, and for Qwen-70B from -0.34 to -0.57, indicating a strong fairness degradation despite preserved utility. Granite-8B and Mixtral-8x7B, exhibit similar changes in SPD_D , suggesting that the downstream classifier only partially attenuates the injected bias rather than eliminating it. Also, we observe that downstream classifiers are especially vulnerable to in-context bias propagation when used for complex

tasks such as Compas and Thyroid, where we argue that the downstream model does not rely on a small subset of predictive features as indicators, and might easily leverage the new introduced adversarial correlations.

We observe analogous trends across datasets in Table 2. In many configurations synthetic data become more biased (e.g., Qwen-70B on Diabetes and Mistral-7B on Adult), and this bias either transfers directly to the downstream classifier or interacts with the model’s own prior biases. Notably, Qwen-70B already exhibits a large baseline disparity on Compas at $\pi = 0$ (with $\text{SPD}_S = -0.51$ and $\text{SPD}_D = -0.40$), and the attack further pushes the model towards extreme group imbalances. We explain this heterogeneity across model families through our propagation analysis in Section 4, where larger or more strongly biased models tend to be easily manipulated via a small number of adversarial demonstrations, and the induced disparities persist when training standard ML models on top of the generated data. Finally, we study in Figure 11 how equal opportunity and equalized odds fairness metrics are influenced by increasing bias rates. We observe an analogous monotonic increase trend, with in-context bias influencing the TPR downstream difference between subgroups.

Utility–fairness trade-off. We can observe in Figure 12 and Table 2 that fairness can deteriorate substantially while conventional utility metrics remain largely unchanged. Across datasets and models, the variation in F1_R between $\pi = 0$ and $\pi = 0.6$ is typically within 0.1 or 0.2. In contrast, the corresponding change in SPD_D can exceed 0.3 for the most affected settings (e.g., Mistral-7B and Qwen-70B on Compas and Adult). Overall, a large fraction of model-dataset pairs are affected by in-context bias injection at moderate and intermediate bias levels ($\pi = 0.3$ or $\pi = 0.6$), while achieving F1 scores that are indistinguishable (or even superior) to the unbiased setting.

Robustness across downstream classifiers. Finally, we investigate whether the propagation of bias is influenced by the choice of downstream classification architecture. Table 4 benchmarks three standard classifiers –Random Forest, Logistic Regression, and Gradient Boosting –against TabPFN [35], a recent transformer-based foundation model that employs in-context learning for tabular prediction. We train each classifier using Compas synthetic data generated by Granite-8b under both unbiased ($\pi = 0$) and adversarially biased ($\pi = 0.6$) conditions. While TabPFN achieves the highest utility (F1_R) among the evaluated models, it remains highly susceptible to in-context bias, exhibiting a significant increase in disparity ($\Delta(\text{SPD}_D) = 0.1$). Notably, while all four classifiers demonstrate improved F1_R scores at $\pi = 0.6$, this utility gain is consistently accompanied by exacerbated downstream disparity. These findings indicate that switching the downstream classifier is insufficient to neutralize biases embedded in the synthetic data. Once the group-wise generative distribution is distorted, both conventional algorithms and modern foundation models systematically inherit, and in some cases amplify, these demographic disparities.

Taken together, these results reveal a new attack surface for LLM-based tabular data generation. An adversary controlling

Table 4: Effect of downstream classifier on bias propagation for Compas (Granite-8B, $k = 80$). For each classifier, we report macro F1 on the real test set (F1_R) and SPD of the downstream predictions on the real test set (SPD_D) at $\pi = 0$ and $\pi = 0.6$.

Classifier	$\pi = 0.0$		$\pi = 0.6$	
	$\text{F1}_R \uparrow$	$\text{SPD}_D \downarrow$	$\text{F1}_R \uparrow$	$\text{SPD}_D \downarrow$
Random Forest	0.58	-0.52	0.61	-0.41
Logistic Regression	0.53	-0.43	0.55	-0.53
Gradient Boosting	0.58	-0.34	0.57	-0.38
TabPFN [35]	0.61	-0.15	0.62	-0.25

a fraction of the in-context examples can substantially alter the group-wise label distribution of the synthetic data, with this manipulation propagating to downstream classifiers evaluated on real data while maintaining standard utility diagnostics. Critically, an ablation study in Appendix B demonstrates that this propagation persists even when prompts contain no explicit instruction to mirror the structure of the in-context examples, indicating that bias transfer is an emergent property of in-context learning rather than an artifact of prompt design. These findings underscore the need to evaluate whether current in-context preprocessing strategies are sufficient to mitigate adversarial bias injection in data generation pipelines.

5.2. Evaluating In-Context Preprocessing Strategies

In this section, we evaluate the robustness of standard in-context defense strategies against bias injection. While recent approaches [21, 24, 25] successfully preprocess in-context examples for a fair LLM-based classification, adversarial biases injected in LLM-based generation might pass undetected. Our goal is to assess whether statistical parity constraints (Fair-SPD), frequency balancing (group balanced) and correlation-based filtering approaches can effectively neutralize the adversarial patterns identified in Section 5, or if the model’s intrinsic priors and high order correlations injected remain undetected.

We evaluate four strategies –correlation-based filtering, Fair-SPD, group balanced, and random subset –to mitigate in-context bias propagation. While Fair-SPD approach enforces marginal fairness, group balanced enforces a fair frequency count across subgroups, and correlation-based filtering drops the most correlated examples to the protected attribute. We assume that there is no access to an external data source, so we consider subsampling as the viable option to select the most appropriate subset of in-context examples for generation. For group balanced and random subset strategies, we set the subset cardinality k^* to the Fair-SPD subset size for a fair comparison.

5.2.1. Balancing Frequency Counts

Balancing subgroup frequency counts has been a traditional way of mitigating representation bias [25, 36] in in-context classification tasks, which arises when the in-context examples for a subgroup do not reflect the actual distribution [37]. This source of bias is particularly challenging in synthetic tabular data generation scenarios where the amount of in-context examples is small (e.g., $k = 80$). For in-context bias mitigation, balancing the frequency count dilutes the influence of an adversary who

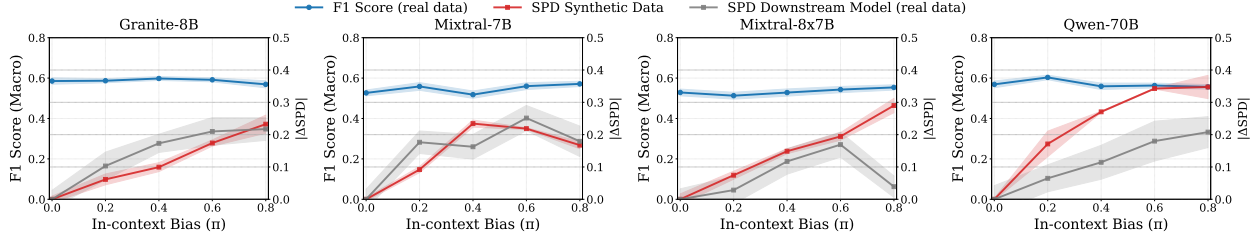


Figure 12: **Adversarial in-context bias injection and utility-fairness trade-off.** (*Compas*) Effect of the in-context bias rate π on downstream performance on real data and fairness for four LLM generators. Each figure shows the macro F1 score of a Random Forest trained on the synthetic data and evaluated on the real test set (blue), the absolute SPD of the synthetic data (red), and the absolute SPD of the downstream predictions on real data (grey). While F1 on real data remains nearly constant as π increases, both synthetic and downstream SPDs grow, showing that small in-context biases can substantially degrade fairness while preserving downstream accuracy.

injects bias only to a specific subgroup, implicitly reducing the bias. For a fair comparison, we set the final subset size of the group balanced mitigation to match the Fair-SPD subset size.

5.2.2. Correlation-based Filtering

We include a correlation-based filtering designed to counter feature-aligned injections by pruning examples that strongly encode dependencies between the protected attribute and other features. We first compute a global correlation weight ρ_j for each feature j with respect to the protected attribute, aggregating Pearson, Spearman, and Mutual Information scores. We then assign a correlation score s_i to each example x_i based on its feature magnitudes weighted by ρ_j : $s_i = \sum_j \rho_j \cdot |z_{i,j}|$ where $z_{i,j}$ is the standardized value of feature j . We filter the prompt by removing examples with the highest s_i (e.g., top 10%), aiming to remove the injected adversarial correlations.

5.2.3. Fair-SPD

We implement a selection algorithm that explicitly controls the statistical parity difference (SPD) of the in-context examples. The goal is to adjust the prompt examples so that their group-level disparity is aligned with a desired target level of fairness (SPD = 0), while discarding as few examples as possible.

Our objective is to identify a subset $\mathcal{S}' \subseteq \mathcal{S}$ derived from the initial pool of $k = 80$ examples that satisfies a group fairness constraint $|\text{SPD}(\mathcal{S}')| \leq \epsilon$, where ϵ represents a predefined tolerance. To achieve this without a computationally expensive exhaustive search, we employ a greedy pruning approach.

Starting with the full set $\mathcal{S}_{curr} = \mathcal{S}$, we iteratively remove the single example that contributes most to the current disparity. At each step t , we identify the optimal candidate x^* for removal by minimizing the SPD of the resulting subset:

$$x^* = \underset{x \in \mathcal{S}_{curr}}{\operatorname{argmin}} |\text{SPD}(\mathcal{S}_{curr} \setminus \{x\})|$$

We update the set via $\mathcal{S}_{curr} \leftarrow \mathcal{S}_{curr} \setminus \{x^*\}$. This process repeats until the stopping criterion $|\text{SPD}(\mathcal{S}_{curr})| \leq \epsilon$ is met, ensuring the final prompt adheres to the desired fairness threshold while retaining the remaining context history.

5.2.4. Experimental Results

We evaluate the mitigation strategies compared to the vanilla biased results ($\pi = 0.3$) following the experimental setup de-

scribed in Section 4.2.1. Before generating synthetic examples, we apply each of the strategies to the in-context examples as a pre-processing step, and then evaluate the resulting dataset once the generation is completed. In Figure 13, we provide a comparison across mitigation techniques for *Compas* and *Qwen-70b* for increasing levels of in-context bias. Here, the target group is African-American, and the target variable is recidivism. As π increases, the synthetic data disparity SPD_S increases under the biased baseline. Random subset selection can partially attenuate SPD_S , but typically remains closer to the biased scenario. Frequency balancing further reduces SPD_S in many settings by correcting representation imbalances introduced by oversampling adversarial examples in the prompt. Fair-SPD keeps SPD_S comparatively stable across π and achieves the lowest downstream disparity SPD_D among the evaluated approaches. However, while enforcing demographic parity in the prompt attenuates marginal bias transfer, SPD_D can still increase with prompt bias π , suggesting that injected bias may propagate through higher-order correlations not captured by marginal parity alone.

Complementing this analysis, Table 5 summarizes mitigation results on *Adult* and *Compas* across four LLMs. Overall, Fair-SPD consistently reduces downstream disparity SPD_D relative to the unmitigated baseline, while preserving comparable F1 in most settings. While improvements in SPD_S are frequent, there are cases where SPD_S does not decrease even when SPD_D improves, indicating a decoupling between synthetic marginal parity and downstream parity. Moreover, fairness gains measured by SPD do not guarantee improvements in EO/EOD, which can remain large or even worsen in some configurations. Taken together, these results indicate that fairness-constrained prompt selection is a stronger baseline than randomization or frequency balancing for limiting downstream bias propagation, but it does not fully eliminate adversarial bias injection across all models and metrics.

6. Discussion

While recent work has established Large Language Models (LLMs) as powerful few-shot tabular data generators, improving downstream performance while avoiding the computational cost of model training, our findings reveal a critical vulnerability inherent to this paradigm. The mechanisms that drive high-fidelity

Table 5: Change in utility (F1 \uparrow), Statistical Parity Difference on the synthetic data (SPD $_S\downarrow$) and downstream model (SPD $_D\downarrow$) after mitigation ($k=80, \pi = 0.3, \epsilon = 0.02$). The cardinality of group-balanced and random subset mitigation subsets are set to the Fair-SPD subset for comparison.

Model	Baseline	Adult					Compas				
		F1 \uparrow	SPD $_S\downarrow$	SPD $_D\downarrow$	EO $_D\downarrow$	EO $_{D\downarrow}$	F1 \uparrow	SPD $_S\downarrow$	SPD $_D\downarrow$	EO $_D\downarrow$	EO $_{D\downarrow}$
Granite-8B	No mitigation	0.73	-0.48 $_{0.02}$	-0.20 $_{0.02}$	0.13 $_{0.03}$	0.19 $_{0.03}$	0.59	-0.25 $_{0.01}$	-0.32 $_{0.03}$	0.29 $_{0.09}$	0.30 $_{0.08}$
	Random subset	0.71	-0.43 $_{0.06}$	-0.20 $_{0.02}$	0.06 $_{0.03}$	0.17 $_{0.04}$	0.60	-0.26 $_{0.05}$	-0.16 $_{0.04}$	0.21 $_{0.07}$	0.25 $_{0.07}$
	Group-balanced	0.74	-0.36 $_{0.02}$	-0.17 $_{0.01}$	0.04 $_{0.02}$	0.11 $_{0.01}$	0.57	-0.21 $_{0.01}$	-0.25 $_{0.04}$	0.34 $_{0.06}$	0.31 $_{0.05}$
	Fair-SPD	0.75	-0.41 $_{0.01}$	-0.15 $_{0.01}$	0.09 $_{0.03}$	0.13 $_{0.01}$	0.60	-0.19 $_{0.02}$	-0.12 $_{0.03}$	0.14 $_{0.07}$	0.15 $_{0.06}$
	Correlation filtering	0.73	-0.44 $_{0.02}$	-0.20 $_{0.01}$	0.06 $_{0.02}$	0.16 $_{0.02}$	0.59	-0.22 $_{0.01}$	-0.18 $_{0.03}$	0.26 $_{0.06}$	0.27 $_{0.06}$
Mistral-7B	No mitigation	0.66	-0.15 $_{0.05}$	-0.11 $_{0.01}$	0.03 $_{0.02}$	0.09 $_{0.02}$	0.53	-0.28 $_{0.01}$	-0.27 $_{0.03}$	0.54 $_{0.07}$	0.48 $_{0.06}$
	Random subset	0.64	-0.03 $_{0.02}$	-0.09 $_{0.01}$	0.02 $_{0.02}$	0.04 $_{0.02}$	0.52	-0.42 $_{0.00}$	-0.23 $_{0.04}$	0.35 $_{0.06}$	0.33 $_{0.06}$
	Group-balanced	0.65	-0.07 $_{0.05}$	-0.09 $_{0.01}$	0.04 $_{0.03}$	0.08 $_{0.02}$	0.53	-0.31 $_{0.03}$	-0.24 $_{0.04}$	0.41 $_{0.09}$	0.43 $_{0.09}$
	Fair-SPD	0.66	-0.00 $_{0.01}$	-0.06 $_{0.01}$	0.08 $_{0.02}$	0.07 $_{0.01}$	0.52	-0.34 $_{0.01}$	-0.19 $_{0.03}$	0.34 $_{0.09}$	0.44 $_{0.09}$
	Correlation filtering	0.65	-0.09 $_{0.01}$	-0.10 $_{0.01}$	0.04 $_{0.03}$	0.10 $_{0.02}$	0.55	-0.46 $_{0.00}$	-0.38 $_{0.03}$	0.62 $_{0.09}$	0.64 $_{0.09}$
Mixtral-8x7B	No mitigation	0.71	-0.27 $_{0.03}$	-0.17 $_{0.02}$	0.05 $_{0.04}$	0.11 $_{0.02}$	0.52	-0.25 $_{0.01}$	-0.27 $_{0.03}$	0.13 $_{0.09}$	0.16 $_{0.07}$
	Random subset	0.71	-0.23 $_{0.01}$	-0.14 $_{0.02}$	0.12 $_{0.03}$	0.11 $_{0.02}$	0.57	-0.33 $_{0.03}$	-0.20 $_{0.03}$	0.33 $_{0.06}$	0.37 $_{0.07}$
	Group-balanced	0.72	-0.20 $_{0.00}$	-0.11 $_{0.01}$	0.14 $_{0.03}$	0.09 $_{0.01}$	0.57	-0.25 $_{0.01}$	-0.15 $_{0.04}$	0.22 $_{0.08}$	0.26 $_{0.08}$
	Fair-SPD	0.73	-0.17 $_{0.01}$	-0.10 $_{0.01}$	0.16 $_{0.03}$	0.10 $_{0.01}$	0.49	-0.22 $_{0.01}$	-0.14 $_{0.03}$	0.19 $_{0.08}$	0.22 $_{0.07}$
	Correlation filtering	0.72	-0.26 $_{0.02}$	-0.13 $_{0.01}$	0.14 $_{0.03}$	0.10 $_{0.01}$	0.54	-0.29 $_{0.01}$	-0.26 $_{0.04}$	0.38 $_{0.06}$	0.40 $_{0.07}$
Qwen-70B	No mitigation	0.73	-0.35 $_{0.04}$	-0.12 $_{0.02}$	0.09 $_{0.03}$	0.13 $_{0.02}$	0.61	-0.72 $_{0.02}$	-0.43 $_{0.02}$	0.39 $_{0.07}$	0.45 $_{0.07}$
	Random subset	0.71	-0.24 $_{0.01}$	-0.13 $_{0.01}$	0.15 $_{0.03}$	0.13 $_{0.01}$	0.55	-0.65 $_{0.03}$	-0.39 $_{0.04}$	0.60 $_{0.09}$	0.57 $_{0.09}$
	Group-balanced	0.71	-0.15 $_{0.02}$	-0.11 $_{0.01}$	0.20 $_{0.02}$	0.17 $_{0.01}$	0.59	-0.56 $_{0.02}$	-0.41 $_{0.03}$	0.46 $_{0.04}$	0.43 $_{0.05}$
	Fair-SPD	0.70	-0.05 $_{0.03}$	0.01 $_{0.02}$	0.36 $_{0.03}$	0.19 $_{0.02}$	0.58	-0.61 $_{0.00}$	-0.36 $_{0.04}$	0.39 $_{0.09}$	0.41 $_{0.09}$
	Correlation filtering	0.73	-0.28 $_{0.05}$	-0.07 $_{0.01}$	0.25 $_{0.02}$	0.14 $_{0.01}$	0.58	-0.64 $_{0.01}$	-0.42 $_{0.03}$	0.57 $_{0.06}$	0.57 $_{0.06}$

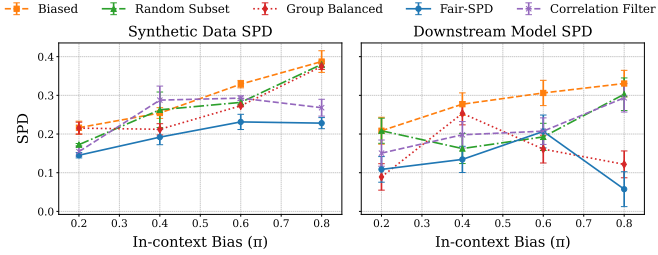


Figure 13: **Synthetic and downstream fairness vs in-context bias π for each mitigation approach.** (*Granite-8b, Compas*) SPD of the synthetic dataset generated by the LLM (left) and downstream classifier predictions on the real test dataset (right) for increasing bias rates across mitigations.

generation are the very same that facilitate bias propagation. Interestingly, while a larger in-context size k allows the model to better capture the in-context distribution, it simultaneously increases the model’s sensitivity to demographic skews. This creates a non-trivial trade-off where increasing the context window to improve synthetic data utility inadvertently heightens the risk of replicating historical injustices or adversarial injections. Furthermore, we demonstrated that the susceptibility to in-context bias is a fundamental property of the learning paradigm itself, rather than a behavior emerging solely from model scale or from prompt engineering.

This mechanism of in-context bias propagation can be exploited by an adversary to maliciously inject biases for a targeted subgroup, even when the target lies at the intersection of multiple variables. We introduced adversarial in-context bias injection as a new vulnerability scheme in LLM-based generation pipelines, showing that it affects fairness in synthetic data while maintaining high utility, rendering the attack invisible to standard utility analysis. While the severity varies by dataset and model, we show that this vulnerability impacts all evaluated models. Furthermore, we demonstrate that these synthetic biases are captured by downstream models, leading to discriminatory

predictions on real test data. This vulnerability persists across various downstream architectures, including traditional classifiers and modern tabular foundation models like TabPFN, which inherit and sometimes amplify the injected disparities.

Finally, we evaluated how in-context pre-processing techniques affect data generation. We observe that balancing the frequency count can mitigate biases by diluting the influence of an adversary injecting examples from a specific subgroup. Similarly, enforcing a fair Statistical Parity Difference (SPD) within in-context examples attenuates adversarial bias injection. However, biases often persist due to the model’s intrinsic priors and the leakage of higher-order correlations that marginal constraints fail to capture. We leave as future work the study of in-processing and post-processing techniques to further mitigate adversarial in-context bias without compromising the utility of the generated data.

7. Conclusion

In this paper, we systematically characterized how statistical biases within in-context examples propagate to LLM-generated tabular data. We demonstrated that as the number of in-context examples increases, the model increasingly aligns with the statistical properties of the prompt, thereby replicating univariate, conditional, and intersectional biases. Building on this, we introduced a novel adversarial framework where a malicious adversary can inject feature-aligned examples to manipulate the output distribution for a targeted subgroup. Our results show that this manipulation compromises fairness without degrading standard utility metrics, creating a stealthy vulnerability that passes undetected by standard diagnostics. Furthermore, we show that these disparities are transferred to downstream classifiers, which often amplify the injected bias. Finally, while we found that in-context pre-processing defenses can attenuate these effects, they are insufficient to fully neutralize the injected bias, highlighting the need for more robust safeguards in generative data pipelines.

Acknowledgements

This work has been partially financed by grant agreement EU-HORIZON GA.101095717 and by grant agreement EU-HORIZON MSCA GA.101086248. Also, it has been partially financed by Generalitat de Catalunya (AGAUR) under grant agreement 2021-SGR-00478, by Severo Ochoa Center of Excellence CEX-2021-001148-S-20-3, and by the Spanish Ministry of Science (MICINN), the Research State Agency (AEI) and European Regional Development Funds (ERDF/FEDER) under grant agreement PID2021-126248OB-I00, MCIN/AEI/10.13039/501100011033/FEDER, UE. Kieran Fraser and Anisa Halimi were partly supported by the Innovative Health Initiative Joint Undertaking (IHI JU) under grant agreement No. 101172997 – SEARCH.

References

- [1] V. Borisov, K. Seßler, T. Leemann, M. Pawelczyk, G. Kasneci, Language models are realistic tabular data generators, arXiv preprint arXiv:2210.06280 (2022).
- [2] L. Xu, M. Skoularidou, A. Cuesta-Infante, K. Veeramachaneni, Modeling tabular data using conditional gan, *Advances in neural information processing systems* 32 (2019).
- [3] Z. Zhao, A. Kumar, R. Birke, L. Y. Chen, Ctab-gan: Effective table data synthesizing, in: *Asian conference on machine learning*, PMLR, 2021, pp. 97–112.
- [4] J. Kim, T. Kim, J. Choo, Epic: Effective prompting for imbalanced-class data synthesis in tabular data classification via large language models, *Advances in Neural Information Processing Systems* 37 (2024) 31504–31542.
- [5] N. Seedat, N. Huynh, B. van Breugel, M. van der Schaar, Curated llm: Synergy of llms and data curation for tabular augmentation in ultra low-data regimes (2023).
- [6] M. Nadeem, A. Bethke, S. Reddy, Stereoset: Measuring stereotypical bias in pretrained language models, in: *Proceedings of the 59th annual meeting of the association for computational linguistics and the 11th international joint conference on natural language processing (volume 1: long papers)*, 2021, pp. 5356–5371.
- [7] E. Dinan, A. Fan, A. Williams, J. Urbanek, D. Kiela, J. Weston, Queens are powerful too: Mitigating gender bias in dialogue generation, in: *Proceedings of the 2020 Conference on Empirical Methods in Natural Language Processing (EMNLP)*, 2020, pp. 8173–8188.
- [8] K. Leino, E. Black, M. Fredrikson, S. Sen, A. Datta, Feature-wise bias amplification, arXiv preprint arXiv:1812.08999 (2018).
- [9] M. Hall, L. van der Maaten, L. Gustafson, M. Jones, A. Adcock, A systematic study of bias amplification, arXiv preprint arXiv:2201.11706 (2022).
- [10] S. M. Tazwar, M. Knobbout, E. H. Quesada, M. Popa, Tabvae: A novel vae for generating synthetic tabular data., in: *ICPRAM*, 2024, pp. 17–26.
- [11] F. H. K. D. S. Tanaka, C. Aranha, Data augmentation using gans, arXiv preprint arXiv:1904.09135 (2019).
- [12] H. Zhang, J. Zhang, B. Srinivasan, Z. Shen, X. Qin, C. Faloutsos, H. Rangwala, G. Karypis, Mixed-type tabular data synthesis with score-based diffusion in latent space, arXiv preprint arXiv:2310.09656 (2023).
- [13] A. Kotelnikov, D. Baranchuk, I. Rubachev, A. Babenko, Tabddpm: Modelling tabular data with diffusion models, in: *International conference on machine learning*, PMLR, 2023, pp. 17564–17579.
- [14] N. V. Chawla, K. W. Bowyer, L. O. Hall, W. P. Kegelmeyer, Smote: synthetic minority over-sampling technique, *Journal of artificial intelligence research* 16 (2002) 321–357.
- [15] Y. Wang, D. Feng, Y. Dai, Z. Chen, J. Huang, S. Ananiadou, Q. Xie, H. Wang, Harmonic: Harnessing llms for tabular data synthesis and privacy protection, arXiv preprint arXiv:2408.02927 (2024).
- [16] M. Tornqvist, J.-D. Zucker, T. Fauvel, N. Lambert, M. Berthelot, A. Movschin, A text-to-tabular approach to generate synthetic patient data using llms, arXiv preprint arXiv:2412.05153 (2024).
- [17] N. Nangia, C. Vania, R. Bhalerao, S. Bowman, Crowspairs: A challenge dataset for measuring social biases in masked language models, in: *Proceedings of the 2020 conference on empirical methods in natural language processing (EMNLP)*, 2020, pp. 1953–1967.
- [18] E. M. Smith, M. Hall, M. Kambadur, E. Presani, A. Williams, "i'm sorry to hear that": Finding new biases in language models with a holistic descriptor dataset, arXiv preprint arXiv:2205.09209 (2022).
- [19] J. Dhamala, T. Sun, V. Kumar, S. Krishna, Y. Puk-sachatkun, K.-W. Chang, R. Gupta, Bold: Dataset and metrics for measuring biases in open-ended language generation, in: *Proceedings of the 2021 ACM conference on fairness, accountability, and transparency*, 2021, pp. 862–872.
- [20] T. Schick, S. Udupa, H. Schütze, Self-diagnosis and self-debiasing: A proposal for reducing corpus-based bias in nlp, *Transactions of the Association for Computational Linguistics* 9 (2021) 1408–1424.
- [21] H. Ma, C. Zhang, Y. Bian, L. Liu, Z. Zhang, P. Zhao, S. Zhang, H. Fu, Q. Hu, B. Wu, Fairness-guided few-shot prompting for large language models, *Advances in Neural Information Processing Systems* 36 (2023) 43136–43155.

- [22] H. Zhou, Z. Feng, Z. Zhu, J. Qian, K. Mao, Unibias: Unveiling and mitigating llm bias through internal attention and ffn manipulation, arXiv preprint arXiv:2405.20612 (2024).
- [23] Y. Liu, S. Gautam, J. Ma, H. Lakkaraju, Confronting llms with traditional ml: Rethinking the fairness of large language models in tabular classifications, arXiv preprint arXiv:2310.14607 (2023).
- [24] V. Cherepanova, C.-J. Lee, N.-J. Akpınar, R. Fogliato, M. A. Bertran, M. Kearns, J. Zou, Improving llm group fairness on tabular data via in-context learning, arXiv preprint arXiv:2412.04642 (2024).
- [25] P. Kenfack, S. E. Kahou, U. Aïvodji, Towards fair in-context learning with tabular foundation models, arXiv preprint arXiv:2505.09503 (2025).
- [26] D. Solans, B. Biggio, C. Castillo, Poisoning attacks on algorithmic fairness, in: Joint European Conference on Machine Learning and Knowledge Discovery in Databases, Springer, 2020, pp. 162–177.
- [27] M.-H. Van, W. Du, X. Wu, A. Lu, Poisoning attacks on fair machine learning, in: International Conference on Database Systems for Advanced Applications, Springer, 2022, pp. 370–386.
- [28] J. Xue, Q. Lou, M. Zheng, Badfair: Backdoored fairness attacks with group-conditioned triggers, arXiv preprint arXiv:2410.17492 (2024).
- [29] A. Asuncion, D. Newman, Uci machine learning repository, <http://archive.ics.uci.edu/ml>, university of California, Irvine, School of Information and Computer Sciences (2007).
- [30] J. Angwin, J. Larson, L. Kirchner, S. Mattu, Machine bias, <https://www.propublica.org/article/machine-bias-risk-assessments-in-criminal-sentencing>, proPublica (May 2016).
- [31] S. M. Xie, A. Raghunathan, P. Liang, T. Ma, An explanation of in-context learning as implicit bayesian inference, arXiv preprint arXiv:2111.02080 (2021).
- [32] M. Panwar, K. Ahuja, N. Goyal, In-context learning through the bayesian prism, arXiv preprint arXiv:2306.04891 (2023).
- [33] J. Xue, M. Zheng, Y. Hu, F. Liu, X. Chen, Q. Lou, Badrag: Identifying vulnerabilities in retrieval augmented generation of large language models, arXiv preprint arXiv:2406.00083 (2024).
- [34] N. Baracaldo, K. Eykholt, F. Ahmed, Y. Zhou, S. Priya, T. Lee, S. Kadhe, Y. Tan, S. Polavaram, S. Suggs, et al., Benchmarking the effect of poisoning defenses on the security and bias of the final model, in: Workshop on Trustworthy and Socially Responsible Machine Learning, NeurIPS 2022, 2022.
- [35] L. Grinsztajn, K. Flöge, O. Key, F. Birkel, B. Roof, P. Jund, B. Jäger, A. Hayler, D. Safaric, F. J. Simone Alessi, M. Manium, R. Yu, A. Garg, J. Robertson, S. B. L. Hoo, V. Moroshan, M. Bühler, L. Purucker, C. Cornu, L. C. Wehrhahn, A. Bonetto, S. Gambhir, N. Hollmann, F. Hutter, TabPFN-2.5: Advancing the state of the art in tabular foundation models (2025).
- [36] J. Hu, W. Liu, M. Du, Strategic demonstration selection for improved fairness in llm in-context learning, arXiv preprint arXiv:2408.09757 (2024).
- [37] N. Mehrabi, F. Morstatter, N. Saxena, K. Lerman, A. Galstyan, A survey on bias and fairness in machine learning, ACM computing surveys (CSUR) 54 (6) (2021) 1–35.

Appendix

This appendix complements the main manuscript with additional experimental results and implementation details:

- Appendix A presents extended results for all model families, validating the findings from Sections 4 and 5.
- Appendix B provides complete prompt templates and demonstrates that bias propagation persists without explicit mirroring instructions.

Appendix A. Additional Experimental Results

This section extends the empirical evaluation from Sections 4 and 5 to three additional model families: Granite-8b, Mistral-7b, and Qwen-70b. These results demonstrate that bias propagation is a universal phenomenon across model architectures, scales, and context window sizes, validating the generality of our main findings.

Appendix A.1. Marginal Bias Propagation

We first examine marginal bias propagation, systematically increasing the representation of the protected group in the in-context examples via the parameter π . Here, we analyze the relationship between the distributional drift of the prompt (relative to the anchor \mathcal{D}_0) and the resulting drift in the generated distribution. Furthermore, we evaluate how the protected group probability in the generated samples aligns with the probability in the in-context examples. For these experiments on the Adult dataset, the protected group is defined as ‘‘Black’’.

Figure A.14 illustrates the distributional drift across the three models. Consistent with the main text, we observe a relationship between the divergence in the prompt ($D_f(\mathcal{D}_P, \mathcal{D}_0)$) and the divergence in the generated data ($D_f(\mathcal{D}_G, \mathcal{D}_0)$).

Qwen-70b exhibits near-perfect replication of prompt statistics, behaving analogously to the Mixtral-8x7b model analyzed in the main text, with a low-variance regression line for gender bias propagation. However, for race bias propagation, the relationship deviates from strict linearity. In contrast, as shown in the Granite-8b and Mistral-7b plots (Figure A.14, Left and Center), while the general linear trend persists, these smaller models exhibit higher variance for gender bias, whereas Granite-8b specifically displays greater linearity for race bias. This suggests that the targeted attribute interacts with the model prior, influencing the magnitude of the drift. However, the right plot shows a strictly linear relationship between the race proportion in the prompt and the generated data across all models, which indicates that even if distributional drift fluctuates, the generated data faithfully preserves the marginal properties of the prompt.

Sensitivity to Context Size. Figure A.15 illustrates the relationship between the protected group probability in the prompt and the generated data as a function of context size k . We observe across all models that as k increases, the generated distribution converges toward the in-context statistics. This confirms that larger context windows improve the LLM fidelity to the prompt, thereby amplifying the propagation of demographic skews.

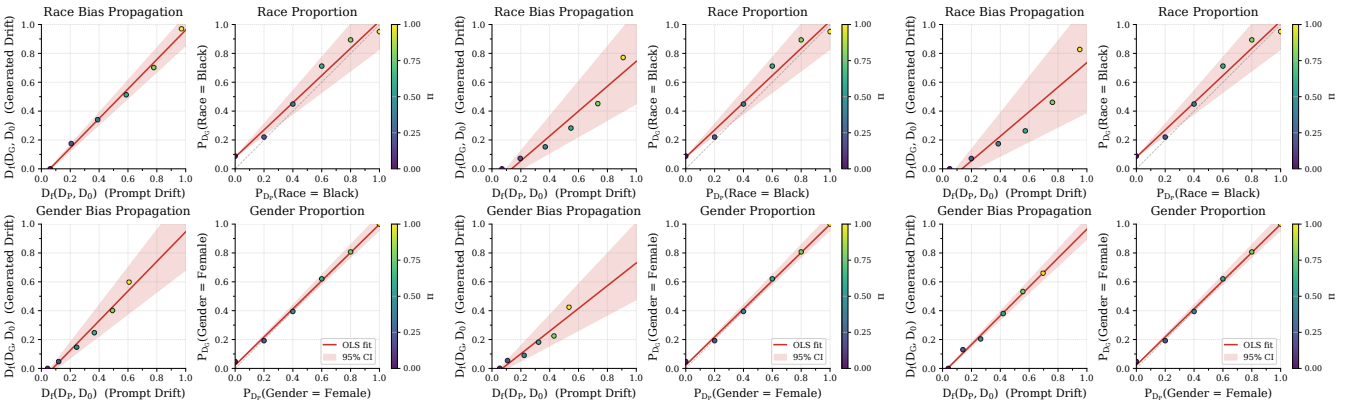


Figure A.14: **Bias propagation across different models.** (Left: Granite-8b; Center: Mistral-7b; Right: Qwen-70b). In all cases, as the bias in the prompt increases, the bias in the generated output scales up linearly.

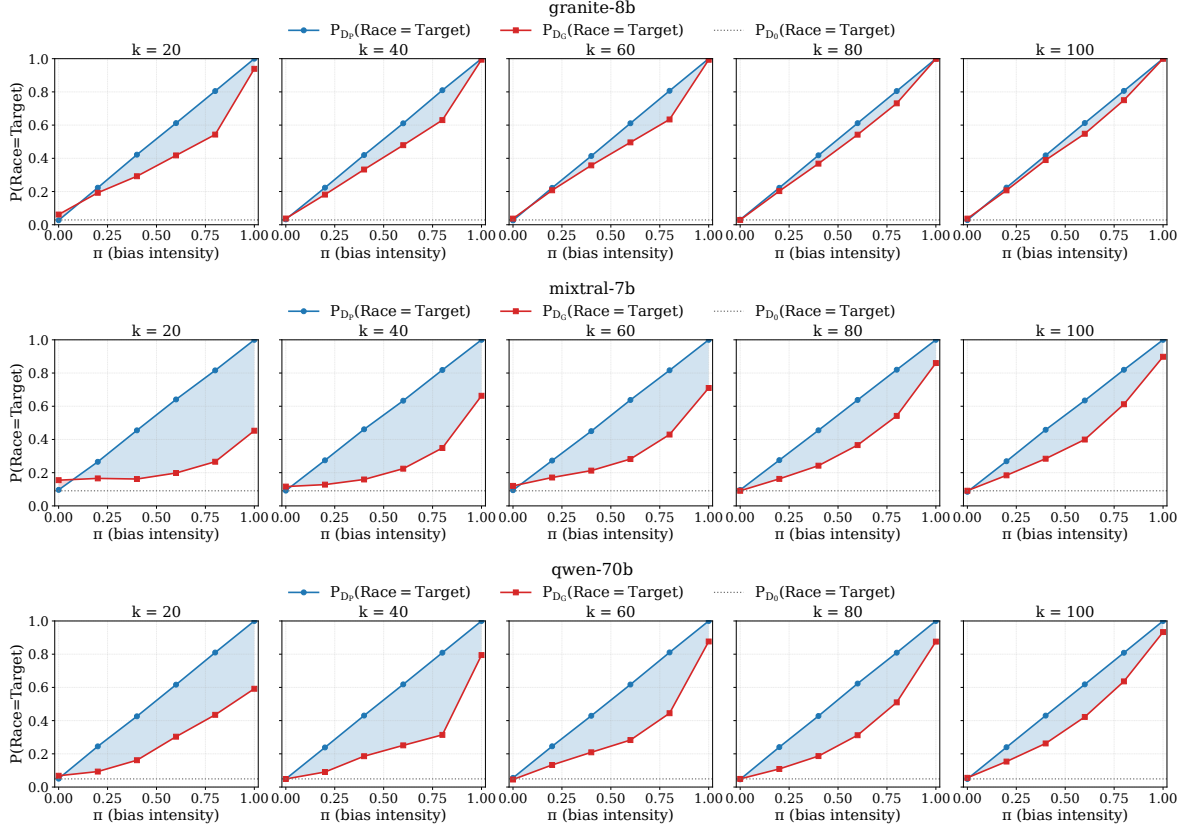


Figure A.15: **Bias propagation strength vs. context size k .** (Top: Granite-8b; Middle: Mistral-7b; Bottom: Qwen-70b). The red curves (D_G) align closer to the blue curves (D_p) as k increases for all models.

Appendix A.2. Conditional Bias Propagation

We further validate the capability of models to isolate bias within a specific subgroup and assess the extent to which this targeted bias leaks into non-targeted demographics. Using the Adult dataset, we systematically bias the Income probability for Female examples while maintaining a fixed probability of 0.5 for Male examples. However, we observe distinct behaviors regarding the non-targeted Male group across different model families. Qwen-70b demonstrates an advanced capability to disentangle conditional distributions $P(Y|X, A)$ from the context, exhibiting minimal leakage to the male subgroup despite the shifting female statistics.

In contrast, smaller models like Mistral-7b display significant bias propagation into the non-targeted group, compared to Mixtral-8x7b within the same family, as observed in Figure 5. This suggests that higher-capacity models achieve greater precision in bias propagation, compared to smaller models within the same architecture and pretraining. Paradoxically, this precision makes the feature-aligned attack described in Section 5 more effective on advanced models.

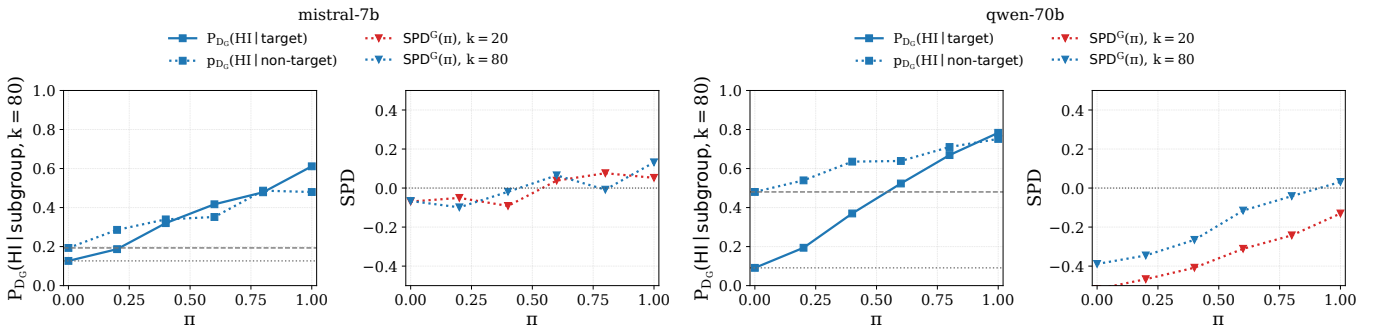


Figure A.16: **Conditional bias propagation on Adult (target: Female).** We systematically vary the in-context Income rate for the Female subgroup while fixing the non-targeted Male subgroup at 0.5 ($k = 80$). While all models correctly propagate the targeted shift, they differ in their ability to isolate this bias. Larger models within the same family (Mixtral-8x7b) demonstrate conditional propagation with minimal spillover to the other subgroup compared to smaller models (Mistral-7b).

Appendix A.3. Adversarial In-Context Bias Injection

Additional feature-aligned analysis. Beyond shifting group-wise label rates, the feature-aligned attacker can also reshape the covariate profile of the targeted subgroup in the synthetic data. For Compas, the attacker anchors highly predictive recidivism features (e.g., `priors_count`, `juv_misd_count`, `juv_other_count`) to plausible values that co-occur with the positive label for the protected group (Table 1). Figure A.17 visualizes this effect by plotting the synthetic univariate densities of aligned predictors separately for African-American individuals and the complementary group as π increases. As the fraction of adversarial examples grows, the protected-group distributions shift toward the attacker’s target region (e.g., mass concentrating around 5 prior counts and near-zero juvenile offenses), whereas the non-targeted group remains closer to its baseline distribution, with minor leak. This separation indicates that the attack is not merely changing marginal outcomes, it induces a subgroup-conditional covariate shift that can make the protected attribute more predictive for downstream models.

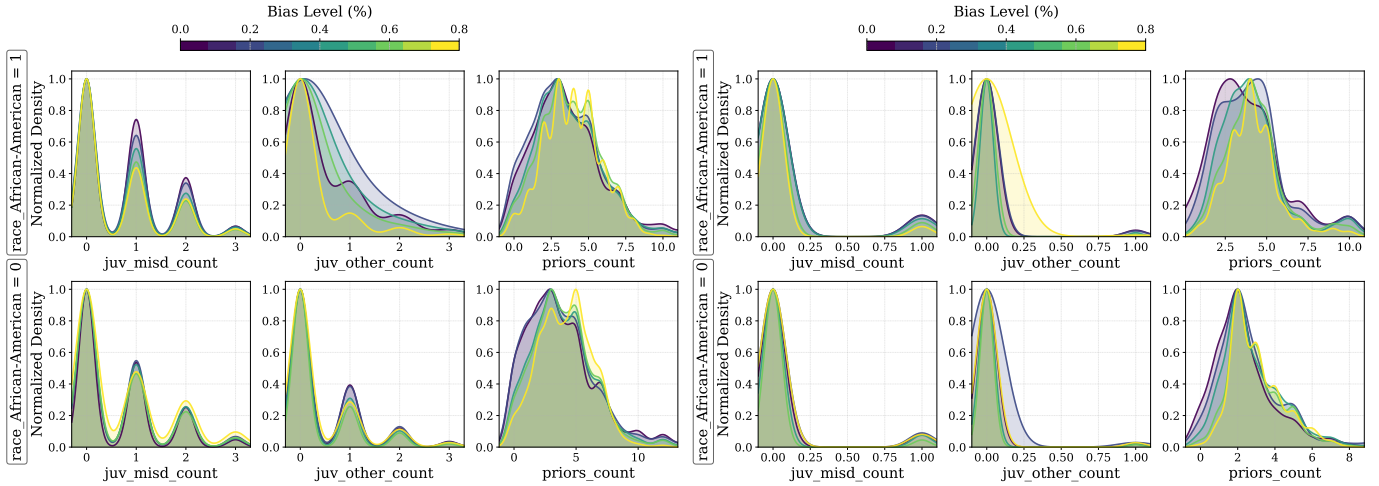


Figure A.17: **Normalized density of aligned features under feature-aligned bias injection.** (*Compas*, $k=80$) Synthetic univariate distributions of key recidivism predictors for the protected subgroup (African-American) and the complementary group as the fraction of adversarial in-context examples π increases. Left: Mistral-7B; right: Qwen-70B. Increasing π steers the protected-group feature profiles toward attacker-chosen plausible values (e.g., lower `priors_count` and fewer juvenile offenses) while leaving the non-targeted group closer to baseline, illustrating the selective subgroup manipulation.

Additional downstream classifiers. Figure A.18 complements the main Random-Forest results by evaluating whether adversarial in-context bias injection remains effective when the downstream learner is changed to Logistic Regression and TabPFN. Across all four LLM generators, increasing the injected bias rate π produces a consistent rise in statistical disparity in the synthetic data (red) and in the downstream predictions evaluated on the real test set (grey), while the macro F1 on real data (blue) stays largely stable. This indicates that once the in-context examples distort the group-conditional label distribution of the synthetic data, both downstream models inherit—and in some cases amplify—these disparities despite similar utility. Overall, these plots reinforce the utility-fairness decoupling observed in the main experiments, where standard accuracy diagnostics alone are insufficient to detect prompt-level fairness attacks in few-shot LLM-based tabular generation.

Appendix B. Prompt Structure

Appendix B.1. Prompt Instruction Ablation

Our main experiments use prompts that explicitly instruct the LLM to "produce realistic yet diverse synthetic samples that mirror the causal structure and feature-label distributions of the provided examples." To test whether bias propagation depends on this explicit mirroring instruction, we conduct an ablation using a minimal prompt: "Using your knowledge of recidivism data, generate exactly two realistic samples." This prompt provides the same in-context examples and output format but offers no guidance about replicating prompt statistics.

We regenerate synthetic data using Mistral-7b and Granite-8b on Compas across π with $k = 80$. Figure B.19 shows that in-context bias propagation persists even without explicit instructions. For both models and both downstream classifiers (Logistic Regression and TabPFN), SPD_S and SPD_D increase substantially with π , while macro F1 remains stable.

These findings demonstrate that bias propagation is an emergent property of in-context learning, rather than a consequence of prompt engineering. Even without explicit instructions to replicate in-context statistics, LLMs implicitly learn and transfer distributional patterns from demonstrations to generated outputs. This has critical security implications, as simply sanitizing prompt instructions is insufficient to prevent adversarial bias injection, as the vulnerability stems from the fundamental mechanism of in-context learning itself.

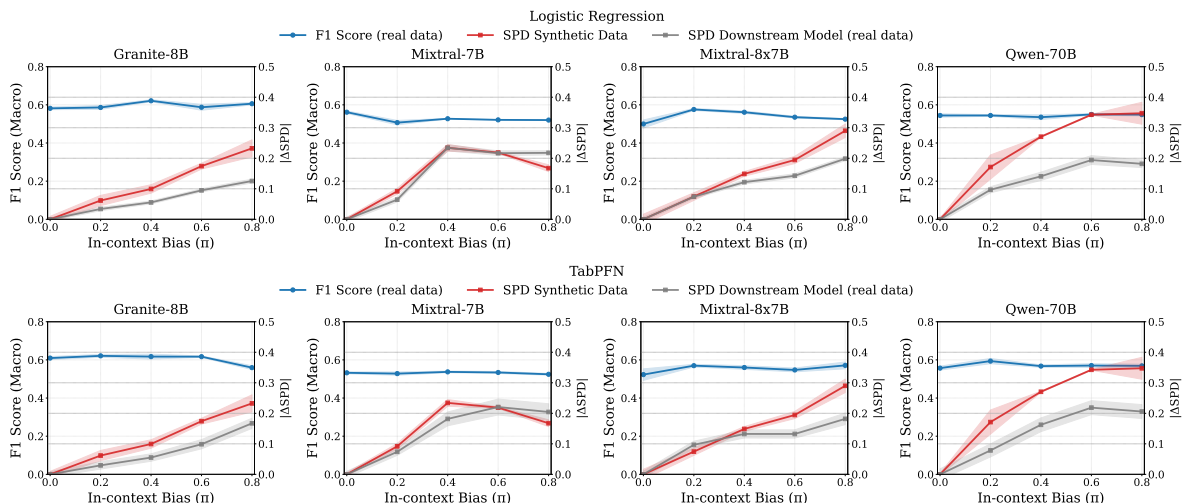


Figure A.18: (*Compas*) Effect of the injected in-context bias rate π on downstream utility and fairness for four LLM-based tabular generators. Top: Logistic Regression; bottom: TabPFN. Curves report macro F1 of the downstream classifier trained on synthetic data and evaluated on the real test set (blue), absolute statistical parity difference (SPD) in the synthetic data (red), and absolute SPD of the classifier’s predictions on the real test set (grey). Across generators and both downstream models, macro F1 remains largely stable as π increases, whereas both synthetic and downstream SPD increase substantially.

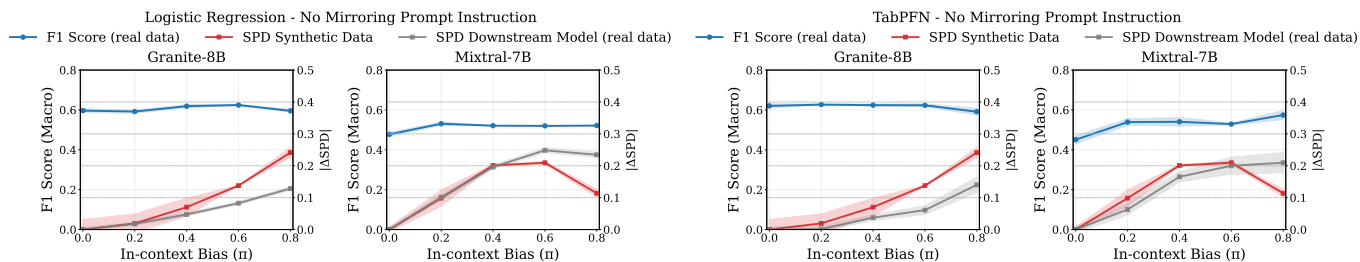


Figure B.19: **Bias propagation persists without explicit mirroring instructions.** (*Compas*, $k=80$) Downstream utility and fairness on real test data for Logistic Regression (left) and TabPFN (right) classifiers trained on synthetic data. Mistral-7b and Granite-8b both show increasing SPD with bias rate π despite stable F1, demonstrating that bias propagation occurs even when prompts contain no instruction to replicate in-context statistics.

Appendix B.2. Prompts Templates

Here we add the prompt templates used for LLM-based tabular generation in our experiments. We include representative prompts for the Adult dataset to clarify (i) the common system role and JSON-format constraints shared across settings, and (ii) the task-specific instructions used in the marginal, conditional, and intersectional analyses. In all cases, the model receives k in-context examples and is required to return a parseable JSON array with a fixed key set and key order. We provide only the changes made over the Marginal Analysis prompt for Conditional and Intersectional prompts.

Unconstrained Prompt – Adult - Marginal Analysis

System role:

You are a tabular synthetic data generator. You produce realistic yet diverse synthetic samples that mirror the causal structure and feature-label distributions of the provided examples.

User instructions:

Using your knowledge of adult income data, generate exactly two realistic samples.
You will first receive a block of real examples as in-context demonstrations:

In-context data:

{icl_examples}

Produce your output as a single JSON array containing two objects. Do not include any explanatory text, commentary, or extra fields. The JSON must be directly parseable (start with [and end with], no trailing commas).

Each object must have exactly these keys in this order:

```
{
  "age": "int",
  "workclass": "string",
  "fnlwgt": "int",
  "education": "string",
  "educational-num": "int",
  "marital-status": "string",
  "occupation": "string",
  "relationship": "string",
  "race": "string",
  "gender": "string",
  "capital-gain": "int",
  "capital-loss": "int",
  "hours-per-week": "int",
  "native-country": "string",
  "income": "string",
}
```

Output example:

```
[
  {example 1},
  {example 2}
]
```

Strict requirement: Return only the JSON array of two objects with the exact key order and no extra keys or prose.

Balanced Prompt – Adult - Conditional Analysis

...

Output example:

```
[
  {example 1 - White},
  {example 2 - Black}
]
```

Strictly return only the JSON array of two objects corresponding to one White and one Black, with same format as the Output example - no prose, no reordered or extra keys.

Balanced Prompt – Adult - Intersectional Analysis

...

User instructions:

Using your knowledge of adult income data, generate exactly four realistic samples—one for each combination of "gender" in {"Female", "Male"} and "race" in {"Black", "White"}:

- ("gender": "Female", "race": "Black")
- ("gender": "Female", "race": "White")
- ("gender": "Male", "race": "Black")
- ("gender": "Male", "race": "White")

You will first receive a block of real examples as in-context demonstrations:

...

Output example:

```
[
  {example 1 - Female - >50K},
  {example 2 - Female - <=50K},
  {example 3 - Male - >50K},
  {example 4 - Male - <=50K}
]
```

Strictly return only the JSON array of four objects corresponding to the four (gender, race) combinations above, with the same format as the Output example - no prose, no reordered or extra keys.

No Mirroring Instruction – Compas

System role:

You are a tabular synthetic data generator. You produce realistic yet diverse synthetic samples.

User instructions:

Using your knowledge of recidivism data, generate exactly two realistic samples.

You will first receive a block of real examples as in-context demonstrations. If this block is empty or missing, proceed anyway using general recidivism priors.

In-context data:

{icl_examples}

...